RAI Volume 3, Chapter 2.2.1.2.1, Second Set, Number 19, Supplemental Question 5:

> Clarify how the maximum static stress drop developed in the RAI response (165 bars) relates to those that DOE suggests account for relatively large ground motions in the PSHA? What is the estimated static stress drop associated with an earthquake on the Solitario Canyon fault or other nearby faults that would produce 407 cm/sec PGV at the site?

1. SUPPLEMENTAL RESPONSE

Although static stress drop is theoretically linked to stress parameter (point-source stress drop), a fundamental factor in determining the level of ground motion, empirical observations show a poor correlation between the two (see the response to Supplemental Question 7). Thus, it is not possible to determine a static stress drop that is directly associated with a horizontal peak ground velocity (PGV) of 407 cm/s at the repository waste emplacement level. Level of ground motion is related to the dynamics of earthquake rupture; water table rise is related to static changes associated with an earthquake.

It is possible, however, to evaluate the consistency of the probabilistic seismic hazard analysis (PSHA) for Yucca Mountain with the screening evaluation of FEP 1.2.10.01.0A, *Hydrologic Response to Seismic Activity*. This supplemental response examines the range of potential water table rise predicted by a bounding representation of the poroelastic response to an earthquake (Kemeny and Cook 1992) that is based on static stress drops and vertical extents of faulting derived from seismic source characterization interpretations and fault displacement hazard developed as part of the PSHA.

A summary of evidence is provided pertaining to water level and water table rise at Yucca Mountain and worldwide observations of earthquake-induced water level and water table rise. Based on a review of the observations of seismic-related water level and water table responses, DOE has concluded that regional stress change models, such as the bounding model developed by Kemeny and Cook (1990, 1992) and a similar model used by the National Research Council, result in a significant overestimation of the potential rise in the water table associated with earthquakes. Taking into account the bounding nature of these models and the available empirical evidence, the supplemental information supports the screening evaluation to exclude FEP 1.2.10.01.0A from the total system performance assessment.

1.1 LACK OF CORRELATION BETWEEN LEVEL OF GROUND MOTION AND STATIC STRESS DROP

In general, observations show a weak dependency of strong ground motions on static stress drop. Conditional on moment magnitude (**M**), strong ground motions over a wide frequency range depend mostly on slip velocity, depth of slip, and source mechanism, all of which may be interrelated. As shown in this section and in the response to Supplemental Question 7, the most robust single parameter that captures relative levels of strong ground motion is the stress parameter ($\Delta\sigma_{SP}$), also referred to as the point-source stress drop or Brune stress drop.

1.1.1 Stress Parameter

Stress parameter controls the point-source corner frequency. Corner frequency is proportional to the inverse of the source size. With respect to the far-field displacement spectrum, it is at the intersection of the relatively constant level at low frequencies and the decreasing level at higher frequencies (Aki and Richards 1981, Chapter 14). For the omega-squared (frequency-squared) source model, the decrease in the level of the displacement spectrum at higher frequencies is proportional to the square of the frequency. For magnitude values that control ground motion hazard at Yucca Mountain (**M** 6 to **M** 7), corner frequency ranges from about 0.30 to about 0.15 Hz (Abrahamson and Silva 2008). The stress parameter is quite sensitive to frequencies from near the corner frequency to as high as those not dominated by nonlinearity at the recording site, or higher if the determination of the stress parameter accommodates potential site nonlinearity (Silva et al. 1996). Stress parameter, conditional on magnitude, is the dominant earthquake source factor controlling strong ground motions at frequencies exceeding the corner frequency.

The stress parameter in the omega-squared source model is defined for the Brune (1970, 1971) circular rupture as (e.g., Silva et al. 1996, Equation 2-3):

$$\Delta\sigma_{SP} = 8.44\,M_0\left(\frac{f_C}{\beta}\right)^3 \qquad \text{(Eq. 1)}$$

in which M_0 is the seismic moment, β the shear-wave velocity in the source region, and f_C the corner frequency.

1.1.1.1 Dependence of the Far-field Acceleration Fourier Amplitude Spectrum on Stress Parameter

The far-field acceleration Fourier amplitude spectrum, $\tilde{a}(f)$, for an omega-squared source model has the following form (Silva et al. 1996, Equation 2-1):

$$\tilde{a}(f) \propto \left(\frac{M_0 f^2}{1+\left(\frac{f}{f_C}\right)^2}\right) \qquad \text{(Eq. 2)}$$

which increases in amplitude as the square of frequency (f) until f_C is reached. For frequencies beyond f_C, the far field acceleration spectrum is constant with a value approximately proportional to:

$$\tilde{a}(f > f_C) \propto M_0\, {f_C}^2 \qquad \text{(Eq. 3)}$$

Solving Equation 1 for f_C and substituting in Equation 3 illustrates the dependence of the source acceleration spectrum on the stress parameter, $\Delta\sigma_{SP}$:

$$\tilde{a}(f > f_C) \propto \Delta\sigma_{SP}^{2/3} M_0^{1/3} \quad \text{(Eq. 4)}$$

Apart from wave propagation effects, e.g. attenuation through the crust and site, the far-field acceleration spectrum for frequencies above the source corner frequency (e.g., about 0.2 Hz for **M** 6.5, Abrahamson and Silva 2008) is directly proportional to the stress parameter, conditional on magnitude (through M_0). Stress parameter is, in effect, a high-frequency spectral scaling parameter with the dimensions of stress.

1.1.1.2 Dependence of Peak Particle Velocity on the Stress Parameter

Considering peak particle velocity (or peak ground velocity) in the context of the omega-squared source model, Equation 2 becomes:

$$\tilde{V}(f) \propto \left(\frac{M_0 f}{1 + \left(\frac{f}{f_C} \right)^2} \right) \quad \text{(Eq. 5)}$$

which has a maximum for the far-field peak particle velocity Fourier amplitude spectrum at frequency f_C that is given by:

$$\tilde{V}(f_C) \propto M_0 f_C \quad \text{(Eq. 6)}$$

Again, solving Equation 1 for f_C and substituting in Equation 6 gives:

$$\tilde{V}(f_C) \propto \Delta\sigma_{SP}^{1/3} M_0^{2/3} \quad \text{(Eq. 7)}$$

Compared to $\tilde{a}(f)$ at high frequency ($f > f_C$), the maximum particle velocity shows a weaker dependence on the stress parameter and a stronger dependence on magnitude (through M_0), due to the contribution of lower-frequency ($f \approx f_C$) amplitudes to the peak particle velocity.

A rough approximation to the time domain value of peak particle velocity based on the Fourier amplitude spectrum is the product of the Fourier amplitude and the bandwidth about the frequency of interest, with the bandwidth typically taken as the frequency of interest (Aki and Richards 1980).

Using this approximation, the peak particle velocity in the time domain becomes:

$$\begin{aligned} V_{max} &\propto M_0 \; f_C^2 \\ &\propto \Delta\sigma_{SP}^{\frac{2}{3}} \; M_0^{\frac{1}{3}} \end{aligned} \qquad \text{(Eq. 8)}$$

and is directly proportional to the stress parameter, conditional on magnitude (through M_0).

1.1.1.3 Dependence of Far-field Acceleration Fourier Amplitude Spectrum on Slip Velocity

The fundamental physical parameter of the earthquake source that controls the corner frequency (f_C), and thereby the stress parameter, is the slip velocity. Since the far-field displacement is directly proportional to the slip velocity (Aki and Richards 1980), the Fourier amplitude spectrum for the slip velocity has the functional form:

$$\dot{U}(f) \propto \left(\frac{1}{1 + \left(\frac{f}{f_C} \right)^2} \right) \qquad \text{(Eq. 9)}$$

with a maximum value at $f = f_C$. The approximate maximum value for the slip velocity in the time domain is then:

$$\dot{U}_{max} \propto f_C \qquad \text{(Eq. 10)}$$

which illustrates that slip velocity fundamentally controls the high-frequency ($f > f_C$) radiation. Substituting Equation 10 into Equation 3, shows that high-frequency far-field acceleration is controlled directly by the maximum slip velocity:

$$\tilde{a}(f > f_C) \propto M_0 \; \dot{U}_{max}^2 \qquad \text{(Eq. 11)}$$

conditional on magnitude (through M_0). Slip velocity, or final slip divided by the rise time, for fixed magnitude, is the dominant single parameter controlling radiation for frequencies exceeding about 0.2 to beyond 25.0 Hz for magnitude about 6.5. This conclusion applies to finite rupture models as well as point-source models, although for finite models any particular site may be dramatically influenced by rupture velocity and rupture directivity, particularly at near-source distances. The controlling aspect of slip velocity, in the case of finite ruptures, refers to general or average site locations.

1.1.2 Stress Parameter and Static Stress Drop

The response to Supplemental Question 7 provides additional discussion of the relation between stress parameter and static stress drop. A theoretical development establishes the linkage between stress parameter and static stress drop within the context of the Brune (1970) source model. Analyses based on ground motions and earthquake data compiled as part of the Next Generation Ground Motion Attenuation (NGA) project show that median stress parameter and median static stress drop are about equal, updating information provided in the original response to RAI 3.2.2.1.2.1-2-019 and Supplemental Questions 1 and 6. However, correlation between static stress drop and stress parameter for individual earthquakes is quite low. The analyses demonstrate that stress parameter is correlated with magnitude, fault mechanism, and the depth over which slip predominately occurs, while static stress drop is not.

While theoretically linked, static stress drop and stress parameter differ in their relation to strong ground motion. Strong ground motion is correlated to stress parameter, which is related to the dynamics of fault rupture. Static stress drop shows a poor correlation to strong ground motion (Section 1.1, Response to Supplemental Question 7). Thus, it is not possible to provide a general relation between static stress drop and strong ground motions determined by the PSHA, nor it is possible to provide a specific value of static stress drop associated with a PGV of 4.07 m/s at the repository waste emplacement level, based on the PSHA.

1.2 WATER TABLE RISE CONSISTENT WITH PSHA SEISMIC SOURCE CHARACTERIZATIONS

Characterizations of maximum magnitude and rupture area (length and down-dip width) for seismic sources in the PSHA are used to calculate static stress drop. The calculated static stress drops and associated vertical extents of faulting are then used to calculate water table rise based on the Kemeny and Cook (1992, Equation 6-1) representation of the poroelastic response of the crust in the vicinity of a normal faulting earthquake. Also, fault displacement hazard with a mean annual probability of exceedance of 10^{-8} for a point on the Solitario Canyon fault is used with rupture area interpretations by the PSHA seismic source characterization teams to calculate a static stress drop. As in the first approach, this static stress drop is used along with the associated vertical extent of faulting to calculate an earthquake-induced water table rise using the bounding Kemeny and Cook (1992, Equation 6-1) representation. When simplifying assumptions that lead to overestimation of water table rise in the bounding Kemeny and Cook (1992) representation (see Section 1.2.1) are taken into account, the results support the screening evaluation that excludes FEP 1.2.10.01.0A, *Hydrologic Response to Seismic Activity*, from the total system performance assessment.

1.2.1 Additional Information Supporting the Screening Evaluation for FEP 1.2.10.01.0A, Hydrologic Response to Seismic Activity

Features, Events, and Processes for the Total System Performance Assessment: Analyses (SNL 2008) provides a screening evaluation for FEP 1.2.10.01.0A, *Hydrologic Response to Seismic Activity*. This screening evaluation addresses the potential for an earthquake-induced water table rise to have a significant impact on the Total System Performance Assessment.

The screening evaluation relies in part on work carried out by a panel of the National Academy of Sciences/National Research Council to assess whether there are plausible mechanisms by which the water table beneath Yucca Mountain could rise to the level of the repository. Consistent with regulations in effect at the time (i.e., 40 CFR 191), the panel assessment was informed by a 10,000-year period of performance following closure of the repository. The panel concluded, "…only a modest rise in the water table of less than 50 m is likely to occur as the result of a nearby earthquake" (National Research Council 1992, p. 116).

The panel conclusion was based on consideration of the poroelastic response of the crust to earthquake-induced volumetric strains. Strains were characterized through a dislocation model approach and through a regional stress change model approach. For the dislocation model approach, strains exhibit a quadrant pattern of volumetric compression and volumetric dilatation. In this model, flow induced by increased pore pressure from volumetric compression tends to migrate to regions of decreased pore pressure associated with volumetric dilatation. Such flow tends to be horizontal and thus does not significantly affect the water table. Modeling of a typical Basin and Range earthquake at Yucca Mountain using this approach (Carrigan et al. 1991; National Research Council 1992, Appendix D) leads to up to several meters of predicted water table rise. Even when input parameters are selected to maximize water table rise (e.g., Carrigan et al. 1991), such models yield results of less than 20 m.

For the regional stress change model approach, volumetric strain is related to the earthquake static stress drop and the mechanical properties of each rock layer. The volumetric strain is considered to be compressive and uniform throughout each layer. The regional stress change model approach does not explicitly model flow, but rather assumes that flow takes place instantaneously and vertically. Water displaced by the compressive volumetric strain is translated to the rock just above the water table where it occupies unsaturated pore space, thus raising the water table. This model is simple, intentionally overestimates water table rise, and allows sensitivities to be quickly tested. Given its charge to assess "the likelihood that the ground water level could rise to the height of the repository by any plausible geological process," the National Research Council panel emphasized the regional stress change model, which gave higher results.

With the promulgation of specific regulations for a repository at Yucca Mountain (10 CFR 63, 40 CFR 197), postclosure performance objectives changed and 10 CFR Part 63 now requires consideration of water table rise past 10,000 years through the period of geologic stability (10 CFR 63.342(c)(1)(i)). In addition, since 1992, scientific investigations have shed new light on ground deformations associated with earthquakes and the relation of hydrologic effects to those deformations.

In response to RAI 3.2.2.1.2.1-2-019 and its Supplemental Questions, the regional stress model of Kemeny and Cook (1992) has continued to be used to demonstrate the consistency of the PSHA and ground motion conditioning work with the screening evaluation excluding FEP 1.2.10.01.0A. While the model is able to quickly provide bounding results, as more extreme seismic events with very low annual probabilities are considered, the bounding nature of the model needs to be clearly considered and its results evaluated in light of its intentional overestimation of water table rise.

1.2.1.1 Background and Introduction

In 1992 a panel convened by the National Research Council completed an evaluation of the possible rise in the water table at Yucca Mountain associated with a nearby earthquake. The principal conclusion reached by the National Research Council panel (National Research Council 1992, p. 116) was:

> The models suggest that regardless of which approach is taken, only a modest rise in the water table of less than 50 m is likely to occur as the result of a nearby earthquake. Although the models are based on very limited data, the panel concludes that stress/strain changes resulting from an earthquake are inadequate to cause more than a few tens of meters rise in the water table based on the convergence of the results of a variety of models and assumptions, especially if the deep carbonate aquifer is as incompressible as the limited data suggest.[1]

This conclusion, which relied primarily on the regional stress change model, was used to support the technical bases for excluding FEP 1.2.10.01.0A, *Hydrologic Response to Seismic Activity*, from the total system performance assessment (SNL 2008, FEP 1.2.10.01.0A). In addition, this conclusion, combined with an inferred correlation developed in the screening justification to exclude FEP 1.2.10.01.0A (SNL 2007, FEP 1.2.10.01.0A) that the maximum 50-m water table rise was due to a 100-bar stress drop, was also used in the responses to RAI 3.2.2.1.2.1-2-019 and Supplemental Question 6.

A review was carried out of some of the research performed since the completion of the National Research Council panel report to determine if the panel analyses are still valid for the intended purpose of determining maximum water table rise following a major earthquake caused by a fault in the vicinity of Yucca Mountain. This review explicitly considers the significant advances in coupled poroelastic effects on geomechanics and hydrology developed in the last 17 years, including direct observations of geomechanical and hydrologic responses to earthquakes and the modeling of such coupled responses.

1.2.1.2 Significant Bounding Assumptions Adopted by the National Research Council Panel

The focus of the analyses performed by the National Research Council panel was to answer the question of whether there are plausible mechanisms, tectonic, thermal, or otherwise, by which the water level at Yucca Mountain could rise to the level of the repository (National Research

[1] The Council, on page 112 of its report, indicates that using the dislocation model "a rise in the water level is thus unlikely." It also states that the dislocation model gives "a water table rise of less than 10 m." The Council panel did its analysis described in the report using the regional stress change model and relegated the dislocation model work of one of its panel members (Bredehoeft) to an appendix of the report. While the conclusion taken alone might be interpreted to mean that both approaches produced similar bounding results, when the details of the discussion of models is examined, it's clear that the panel was led to the value of a 50 m bound by the regional stress change model, not the dislocation model.

Council 1992, Section 1). Given that charter, with respect to seismic mechanisms, the panel focused on providing a seismically induced maximum water table rise associated with a seismic event that the panel believed would not be exceeded. That is, the analysis was meant to provide an upper bound on the estimate of potential water table rise. This is evidenced by the observation that although two different models of possible water level changes associated with poroelastic deformation were postulated in the National Research Council panel report (i.e., the dislocation model and the regional stress change model) the bounding result was produced using the regional stress change model. The degree of conservatism in the National Research Council panel results and conclusion can be evaluated by examining the assumptions within the regional stress change model.

The regional stress change model used by the National Research Council panel to develop a bound on the water table rise is noted as being analogous to the model proposed by Kemeny and Cook (1990), which was later used by Cook and Kemeny (1991) and Kemeny and Cook (1992) to evaluate potential water table rises. As noted by Kemeny and Cook (1990, p. 5-14):

> The approach taken here is to make a series of conservative assumptions to reduce the complex coupled problem to a simple mechanical model. By ensuring that all assumptions are conservative, the results from the model should represent an upper bound on the rise in the water table due to an earthquake of a specified size.

Several key assumptions presented by Kemeny and Cook (1990) are relevant to the determination of the degree of conservatism in the predicted bound of the water table rise; with the most significant assumptions being the following:

- All water displaced from the volume due to coseismic stress change goes up the stratigraphic column instantaneously.

- The coseismic stress change following an earthquake is uniform with depth (Kemeny and Cook 1990, p. 5-15).

The first assumption results in immediately propagating the fluid volume released from the rock compression to the water table and is an upper bound on the water level change. Phenomena that will reduce the amplitude of the change include time-dependent flow, flow directions other than upward, and impermeable beds. While water level changes can occur rapidly in open boreholes intersecting areas of compressed or dilated rock following poroelastic deformation due to an earthquake, the propagation of these changes to the water table is much less pronounced. Essentially, the excess pore pressure would be dissipated in the more permeable rock units and is not propagated vertically through aquitards and low permeability stratigraphic units to the water table surface.

The second assumption appears not to be applicable based on observed deformations associated with fault displacements, as some areas are observed to undergo dilation (thus potentially lowering the observed water level for any wells intersecting these zones) and others compression (thus potentially raising the observed water level for any wells intersecting these zones). That is,

the coseismic poroelastic strains do not appear to be constant with depth, but instead have three-dimensional patterns consistent with poroelastic deformation models of fault displacement.

The combined information of scientific bases and direct observations lead to the conclusion that, although local water level rises in the confined aquifers under Yucca Mountain may experience potentially significant water level changes (if wells penetrated these aquifers), water table rises at Yucca Mountain are expected to be significantly less than the bounding value generated, assuming the regional stress change model of Kemeny and Cook (1990), even under extreme maximum fault displacements along either the Solitario Canyon or Paintbrush Canyon fault.

1.2.1.2.1 Regional Stress Change Model versus Dislocation Model

The National Research Council investigated two models of stress change following an earthquake, a dislocation model and a regional stress change model. The dislocation model "models strain in the traditional way" (National Research Council 1992, p. 112) giving a quadrantal pattern of dilation and compression on opposite sides of the fault. This model was used in analyses performed by Carrigan and King (1991) and Bredehoeft (National Research Council 1992, Appendix D). The regional stress change model considers normal faults in regions of extension (such as the Basin and Range region around Yucca Mountain). During an earthquake, the release of horizontal tension causes a regional increase in horizontal compressive stress and, because of the large regional extent, it is assumed the water squeezed out can only move upward, thus raising the water table (National Research Council 1992, p. 112). This model was used in analyses performed by Cook and Kemeny (1991) and Kemeny and Cook (1990, 1992). As noted by the National Research Council panel, "the difficulty with the dislocation model is that it does not yield a regional change in the state of stress," and "a rise in the water table is thus unlikely" (National Research Council 1992, p. 112).

The National Research Council panel took as their charter an assessment of the likelihood that the ground water level could rise to the height of the repository by any plausible geologic process (National Research Council 1992, pp. 2-3). For earthquake-induced water table rise, the focus of their efforts was on evaluating a possible maximum rise in 10,000 years considering the information available to them, rather than evaluating the likely rise and the uncertainty in that rise. Because they were focused on the maximum rise, it is understandable that they focused on the model that provided the maximum rise: the regional stress change model.

While it is possible to consider the differences in the two models to be one of scale, wherein predicted dislocation-induced strains may be extensive over a large area away from the fault (km to tens of km, see below) or over a large depth, the distinction is in the variability of the strains in the two conceptual representations. In the regional stress change model, only compressional strain is generated and it is assumed that the entire vertical column of rock experiences the same strain. Alternatively, in the dislocation model there is a well understood pattern of compression and dilation depending on location with respect to the fault with strain varying laterally and vertically. Considering the analyses of dislocation-induced strain predicted by Bredehoeft (National Research Council 1992, Appendix D, Figure 2) and Carrigan et al. (1991, Figure 1) for a 1-m offset along a normal fault typical of the Basin and Range region around Yucca Mountain, the lateral extent of the zone of compression nearest the surface (in the footwall) is equivalent to

the depth of the fault (10 km), and the vertical extent of this zone of compression is about 4 km. More important, this zone of compression does not have as large a volumetric strain as locations near the fault tip (for example Bredehoeft predicts a maximum volumetric strain of about 100 microstrain units (or 10^{-4} m^3/m^3) near the fault tip and about 10 microstrain units (or 10^{-5} m^3/m^3) in the area of compression nearer the surface).

A review of recent literature on poroelastic responses of geologic media to earthquakes indicates that the preponderance of the research confirms that strain caused by fault displacements during earthquakes can reasonably explain observations of zones of bulk rock compression and dilation, and that these zones can be related to elastic deformation theory. In addition, this same research indicates that water levels in wells within the zones of compression tend to rise while water levels in wells within zones of dilation tend to fall as expected given the poroelastic theory, although this generalization is not always observed as many competing complexities can affect the direction of water level change at any particular well in the area. (Note: The distinction between water level change and water table change is discussed later). Literature sources evaluating coseismic poroelastic deformation and associated water level changes are summarized by Roeloffs (1996) and Manga and Wang (2007).

Earthquakes in June 2000 along two right-lateral strike slip faults in southern Iceland were shown to exhibit coseismic deformation consistent with a dislocation model, with upward ground movement associated with coseismic extension zones northeast and southwest of the fault and downward ground movement associated with coseismic compression zones northwest and southeast of the fault (Jonsson et al 2003, Figure 2). In addition, predicted coseismic pore-pressure response was shown to reasonably reproduce the observed water level changes in nearby geothermal wells, with areas of water level rises being associated with zones of compression and water level declines being associated with zones of dilation (Jonsson et al. 2003, Figure 3).

A fault model of coseismic strain associated with fault displacement was shown to reasonably correlate to observed groundwater level changes associated with the 2003 Tokachi-oki earthquake. Water level changes in wells in areas of predicted dilation were observed to decrease, while water level changes in wells in areas of predicted contraction were observed to generally increase (Sato et al. 2004, Figure 1).

Observations of step-like coseismic groundwater level changes in confined aquifers were also correlated to the poroelastic response of static strains caused by the 1994 earthquake near Parkfield, California (Quilty and Roeloffs 1994). These authors also concluded that the strains predicted by a dislocation model of the rupture were in good agreement with the changes in most of the wells. Similarly, in an analysis of water level responses following an earthquake at Roermond, Netherlands, it was observed that the water-level response was in general agreement with volume strains (compression or dilation) predicted by poroelastic theory, with 16 of 19 wells with rising water levels corresponding to areas of compression and 7 of 9 wells with water level drops corresponding to areas of dilation, although the magnitudes and durations were larger than expected (Grecksch et al. 1999).

The above references are indicative that scientific evidence since the completion of the National Research Council panel report supports the conclusion that poroelastic strains induced by faulting are reasonably predicted using a dislocation model that has spatially variable strains that can be either compression or dilation of the rock mass associated with the event, and that these strains are able to, in many cases, explain observed water level responses in confined aquifers.

1.2.1.2.2 Vertical Propagation of Water Level Changes to the Water Table

The two models investigated by the National Research Council panel resulted in two different approximations for pore pressure and water level responses in the strained region. In the regional stress change model, because the compression was assumed to be regionally extensive and vertically the same through the section, the water level change at any one point would be considered to be the same. That is, for every cubic meter of rock in the vertical column from the water table to the depth of the assumed fault, the same amount of deformation was assumed and the volume of water associated with the vertical compression of the entire 10-km column was made immediately available to raise the water table.

In contrast, in analyses performed by National Research Council panel member J. Bredehoeft using the dislocation model (National Research Council 1992 Appendix D), although hydraulic head changes associated with the fault displacement may be up to 180 m of head at depths of 9 km, the water table rise was on the order of 1 m. Hydraulic head changes (related to pore compression and associated pore pressure increases) are what one might expect to observe as a water level change if there was an open piezometer at depth in the compressed zone and one did not consider the storage of the well bore. However water table changes are very different than water level changes as discussed below.

1.2.1.3 Observed Water Level and Water Table Rises due to Earthquakes

Documented observations of water level responses that are interpreted to result from earthquake-induced poroelastic deformation generally are from open boreholes, where these water level responses are reflective of the change in pore pressure associated with the deformation. Groundwater level changes may be associated with changes in hydraulic head when the well is open to a confined aquifer(s) or to water table elevation changes when the well is open to an unconfined aquifer. When wells are open to multiple aquifers, the water level in the well will be controlled by the hydraulic head in the most transmissive unit(s) intersecting the well.

The observed water level responses presented in Section 1.2.1.2.1 are generally related to water level responses in confined aquifers. Although researchers have generally not focused on water level responses in comparison to water table responses, the available information supports the conclusion that water table responses are generally much less (in several cases an order of magnitude less) than water level responses.

Coseismic water level responses in wells completed in confined aquifers following the 1999 M_W 7.5 Chi-Chi earthquake in Taiwan were observed to range from less than 1 m to more than 5 m, while water level changes in the uppermost unconfined aquifer were shown to be much smaller (ranging from 0 to 0.5 m) (Manga and Wang 2007, p. 302). In addition, most of the observed

water level changes in wells completed in confined aquifers following the 2003 Tokachi-oki M_W 8.0 earthquake in Japan could be explained by the poroelastic response and volumetric strain derived from a fault dislocation model, while an earlier earthquake in the same area had responses that could not be explained by poroelastic response because it included responses of unconfined aquifers, which are not highly sensitive to volumetric strain changes (Koizumi et al. 2005).

The reason for the greater amplitude of response of the water level in confined aquifers is the result of the smaller storativity of confined aquifers. Considering a given poroelastic compression with the resultant volume of water released per unit surface area of the aquifer, the smaller storativity of the confined aquifer will result in a higher water level rise in boreholes that are open to the confined aquifer. In the vicinity of Yucca Mountain, the Death Valley Regional Groundwater Flow Model has estimated the specific storage of confined aquifers of between 10^{-7} and 10^{-4} m^{-1} and a specific yield of unconfined aquifers of about 0.1 (Belcher 2004, Figure F-38). Considering confined aquifer thicknesses of about 10^2 m implies a storativity of between about 10^{-5} and 10^{-2}, a factor of 10^4 to 10^1 less than the specific yield of the unconfined aquifers. Therefore, an earthquake capable of causing a water level rise of 10 m in the confined aquifers at Yucca Mountain would be expected to cause only a 1.0 to 0.001 m rise in the water table.

The distinction between water level rise and water table rise becomes relevant when confining units separate the aquifers. If there are no confining units, the water table response will be equal to the water level response to the poroelastic deformation, although the time it takes to propagate from the deeper zones to shallower water table is a function of the vertical hydraulic diffusivity of the rock mass (Roeloffs 1996, p. 167). Kemeny and Cook (1990, 1992), in reducing the coupled hydro-mechanical response to a simplified mechanical representation, assumed no confining units and that hydraulic head changes at depth instantaneously propagated to water table elevation changes. In assuming there were no confining units, Kemeny and Cook (1992) effectively assumed that the water volume released by the compression of the entire saturated thickness of rock (about 10,000 m) became available for raising the water table. While this assumption is consistent with development of a bounding model, observations of water level and water table elevation changes noted above, combined with the known confining units in the saturated zone in the vicinity of Yucca Mountain, indicate this assumption results in an overestimation of realistic water table rise values.

1.2.1.4 Possible Seismic-Induced Water Table Fluctuations in the Vicinity of Yucca Mountain

The historical record of water table elevations in the vicinity of Yucca Mountain shows no evidence of past significant rises in the water table associated with seismic events. The observed indicators of previous higher water table elevations and spring discharge elevations are very well correlated with times of previous wetter climates; there is no indication of higher water levels that cannot be reasonably explained by the local effects of a wetter climate. However, water table rises associated with poroelastic deformation due to fault displacement are generally short lived (time periods of months), so observations of such water table rises would not be expected in the geologic record.

Large excursions in the water table resulting from earthquakes in the geologic past could have left evidence of their occurrence in the form of secondary mineral veins. However, multiple lines of evidence from shallow vein minerals and from the deeper unsaturated zone do not indicate that such minerals precipitated from upwelling groundwater from the saturated zone.

There is no evidence from the isotopic geochemistry of shallow calcite veins for large-scale rise in the water table near Yucca Mountain in the geologic past. Stable isotopes of carbon and oxygen from groundwater and calcite veins at Trench 14 and Busted Butte indicate that the calcite could not have precipitated from saturated zone groundwater (National Research Council 1992, Appendix A). Overlap in the carbon and oxygen isotopic compositions of vein calcites and calcite from soils suggest that shallow vein calcites are pedogenic in origin and precipitated from downward percolating infiltration. Differences in the uranium activity ratios in groundwater and shallow calcite veins also preclude upwelling groundwater as the source of these calcite veins. Similarly, discrepancies in the strontium isotopic composition of groundwater and the shallow calcite veins show that this calcite did not precipitate from groundwater in the saturated zone (National Research Council 1992, Appendix A). The National Research Council study concluded (National Research Council 1992, p. 134):

> …the isotopic evidence now available indicates that no prolonged excursion of the water table above its present level has occurred in the last ca. 100 ka.

There is also no evidence of upwelling groundwater from the saturated zone, for at least the last several million years, based on the stable isotopic geochemistry, fluid inclusions, and texture/morphology of secondary calcite and silica from the Exploratory Studies Facility. The carbon and oxygen isotopic compositions of late-stage calcite from the unsaturated zone show little overlap with the range of compositions that could have formed by precipitation from groundwater in the upper saturated zone (National Research Council 1992, Appendix A). Temperatures at the repository horizon have not been impacted by upward flow of warmer groundwater from the saturated zone over the past several million years. Data from fluid inclusion assemblages and integrated uranium-lead age dating from secondary minerals indicate that ambient temperatures have prevailed for approximately the past two to five millions years (Wilson et al. 2003; Whelan et al. 2008). Textural and physical evidence indicate that secondary calcite and opal coatings formed under unsaturated flow conditions with slow, uniform growth rates (Paces et al. 2001).

1.2.1.5 Observed Seismic-Induced Water Level Fluctuations in the Vicinity of Yucca Mountain

Water levels in wells in the vicinity of Yucca Mountain have been observed to change due to coseismic deformation (compression or dilation) associated with nearby earthquakes. Of principal note are the water level responses observed following the June 1992 earthquakes at Landers, California (a M_W 7.6 earthquake that occurred on June 28, 1992, about 300 km southwest of Yucca Mountain), Big Bear Lake, California (a M_W 6.6 earthquake that also occurred on June 28, 1992, about 300 km southwest of Yucca Mountain) and Little Skull Mountain, Nevada (a M_W 5.6 earthquake that occurred on June 29, 1992, about 23 km from Yucca Mountain), and the October 1999 earthquake at Hector Mine, California (a M_W 7.1 about

20 km to the northeast of the Landers earthquake). Short-term fluid pressure oscillations in wells USW H-5 and H-6 associated with the passing seismic waves of the June 1992 earthquakes are illustrated and discussed by O'Brien (1993). In addition, water level offsets, believed to be due to poroelastic deformation of the rock mass, in wells UE-25p#1 and USW H-3 are illustrated in the report by O'Brien (1993), with a decline of about 50 cm in UE-25p#1 (completed in the confined lower carbonate aquifer) and an increase of 28 cm in USW H-3 (completed in a confined tuff aquifer). The location of these and other observation wells discussed below are identified in *Water-Level Data Analysis for the Saturated Zone Site-Scale Flow and Transport Model* (BSC 2004, Figure 1-2). Similar water level offset observations are observed for well AD-4a (with a water level rise of about 3 ft for the Landers/Little Skull Mountain earthquakes and also about 3 ft for the Hector Mine earthquake). In addition, analyses of water level changes at Devils Hole indicate about a 0.1 to 0.04 m decline following the Landers/Little Skull Mountain and Hector Mine earthquakes, respectively (Cutillo and Ge 2006, Figure 3).

With the exception of the above Devils Hole observations (which indicate a decline in the water table surface following the earthquake), the other observations of water level fluctuations are within confined aquifers. Due to the low storativity of the confined aquifers, it is expected that observation wells, piezometers or pressure transducers that are measuring water level changes in these confined aquifers would represent a change that is not reflective of the change in the water table surface, due to the large specific yield of the water table aquifer. To evaluate this, the National Water Information System of the U.S. Geological Survey database of groundwater levels in the vicinity of Yucca Mountain was searched for wells with recorded water levels around the time preceding and immediately following the June 1992 earthquakes. The following observation wells, which are wells that intercept the water table, indicate no discernible change due to these earthquakes: UE-25 WT-17, UE-25 WT-16, USW WT-10, UE-25 WT-14, UE-25 WT-13, USW WT-7, USW WT-1, J-13, and J-12. Well UE-25 WT-4 had about a 1-ft water level increase that quickly dissipated and may even have been an anomalous reading as the data are indicated as being provisional and subject to revision. Well UE-25 WT-6 had about a 3.5 ft increase followed by a decline over about 3 months to a water level that is about 2 ft below the static level before the earthquake. The anomalous behavior at well UE-25 WT-6 may be due to vertical and lateral confinement of this zone which is completed in the low permeability confining unit. Regardless of the explanation of the anomalous behavior at well UE-25 WT-6, the water table response is significantly less than the response in confined aquifers in the area due to the same seismic event. This observation is expected and is consistent with the larger storage in the unconfined aquifers as opposed to the low storativity in the confined aquifers. It reinforces the previously noted general observations that water level responses of the water table are much less than the water level response in wells or piezometers open to confined aquifers.

1.2.1.6 Conclusions

Based on a review of the observations of coseismic water level and water table responses, DOE has concluded that the regional stress change model developed by Kemeny and Cook (1990, 1992) and adopted by the National Research Council (1992), while bounding, results in a significant overestimation of the potential rise in the water table associated with earthquakes affecting Yucca Mountain. In particular, there are two principal areas in which the model is unrealistic and inconsistent with the expected water table response following an earthquake:

- The regional stress change model treats strains from normal faulting in an extensional tectonic regime as resulting in a uniform increase in compressive stress throughout the affected volume of rock. Observations since the model was developed and used by Kemeny and Cook and the National Research Council indicate that strains vary spatially and are well predicted by the dislocation model. Predictions of water table rise based on the regional stress change model, therefore, are overestimated, in part because of the unrealistic characterization of earthquake-induced strain.

- Water table response due to the earthquake-induced uniform compressive strain assumed in the regional stress change model is assumed to lead to uniform pore pressure changes that are immediately propagated vertically through the hydrostratigraphic column with a resultant immediate displacement of the water table surface into the available empty pore space above the water table. In addition to ignoring flow in directions other than vertical, which would result from a more realistic characterization of earthquake-induced strains, this assumption also leads to overestimation of water table rise by not taking into account the effect of confining units, which are known to exist in the Yucca Mountain vicinity.

As a result, estimates of potential water table rises based on the Cook and Kemeny regional stress change model, while bounding, significantly overstate the potential and amplitude of a seismically-induced water table rise.

1.2.2 Estimates of Potential Water Table Rise Based on PSHA Seismic Source Characterization Interpretations

Kemeny and Cook (1990, Section 5.3) developed a simple mechanical representation (Kemeny and Cook 1992, Equation 6-1) to bound earthquake-induced water table rise for a poroelastic model. In this simple representation, water table rise (Δw, meters) is related to earthquake static stress drop ($\Delta\sigma_{static}$, bars) and vertical extent of faulting (h, meters):

$$\Delta w = 1.2 \times 10^{-5} \times \Delta\sigma_{static} \times h \qquad \text{(Eq. 12)}$$

In the responses to RAI 3.2.2.1.2.1-2-019 and Supplemental Questions 1 and 6, the National Research Council (1992, p. 116) conclusion of a bounding 50-m water table rise was incorporated in the use of the Kemeny and Cook representation by adjusting the Kemeny and Cook relation to give a water table rise of 50 m for a 100 bar static stress drop and a 10 km vertical extent of faulting. That is, the 1.2×10^{-5} constant in Equation (12) was assumed to be 5×10^{-5} (i.e., 50-m water table rise = (5×10^{-5}) × (100 bar static stress drop) × (10,000 m vertical extent of faulting)). As this response to Supplemental Question 5 considers even more extreme static stress drops than 100 bars, the upward adjustment that was earlier added to the model is dropped. Thus, in this response, Equation 12 is used as originally developed by Kemeny and Cook (1992). Implications for the earlier RAI and Supplemental Question responses are discussed in Section 1.2.4.

During the PSHA, six three-member teams of experts characterized seismic sources contributing to ground motion and fault displacement hazard at the site. For fault sources, the characterization included interpretations of fault rupture length, down-dip width, and maximum moment magnitude ($\mathbf{M_{max}}$) (CRWMS M&O 1998, Section 4). In this section, these interpretations are used to calculate a static stress drop associated with the largest event on a given fault source. "Local" faults, as identified by the PSHA expert teams, are evaluated for the potential of future water table rise. These faults are within about 20 kilometers of the site and extend from the Bare Mountain fault on the west to the Paintbrush Canyon fault on the east. For one team, the Bare Mountain fault was considered a regional fault, but it is included in this analysis for consistency with the other teams.

Kanamori and Anderson (1975) noted that static seismic moment (M_0) is related to fault rupture area (S), static stress drop ($\Delta\sigma_{static}$), and a characteristic fault dimension (D) as follows:

$$M_0 = \left(D/C\right) S\, \Delta\sigma_{static} \qquad \text{(Eq. 13)}$$

in which C is a non-dimensional shape factor. Using the relation between M_0 (dyne cm) and moment magnitude (**M**) (Hanks and Kanamori 1979, Equation 7):

$$M = \left(2/3\right)\log M_0 - 10.7 \qquad \text{(Eq. 14a)}$$

or equivalently:

$$\log M_0 = 1.5M + 16.05 \qquad \text{(Eq. 14b)}$$

and solving for $\Delta\sigma_{static}$, Equation 13 becomes:

$$\Delta\sigma_{static} = \left(C/D\right)\frac{10^{(1.5M+16.05)}}{S} \qquad \text{(Eq. 15)}$$

Representing the fault rupture as circular, D equals radius (a) and C equals $\left(7\pi/16\right)$. Substituting and replacing S by πa^2, yields:

$$\Delta\sigma_{static} = \left(7/16\right)\frac{10^{(1.5M+16.1)}}{a^3} \qquad \text{(Eq. 16)}$$

For a in centimeters, static stress drop is in dyne/cm^2. To convert to bars, for consistency with the Kemeny and Cook (1992) representation, the stress drop in dyne/cm^2 must be divided by 10^6. This relation is used to relate seismic source characterization results from the PSHA to static stress drop.

Characterization of rupture dimensions and $\mathbf{M_{max}}$ for seismic sources considered in the PSHA included an assessment of uncertainty in those values. Distributions for rupture length are based

on surface geologic mapping and paleoseismic data from trenches excavated across some of the faults. Uncertainty in down-dip rupture width takes into account uncertainty in fault dip and in the vertical extent of the seismogenic zone, the depth to possible detachment structures, or to truncation by other faults. Uncertainty in $\mathbf{M_{max}}$ is assessed by using multiple empirical approaches that relate magnitude to fault characteristics such as rupture length, rupture area, surface displacement, and long-term slip rate. The distribution of $\mathbf{M_{max}}$ for a given fault source varies according to the combination of rupture length and down-dip width on which they are based. Contributions to the distribution of $\mathbf{M_{max}}$ based on displacement or slip-rate data, however, are included for all combinations of rupture length and down-dip width. Thus, if a displacement value for a fault leads to a large $\mathbf{M_{max}}$, the overall distribution of $\mathbf{M_{max}}$ reflects that contribution even for combinations of rupture length and down-dip width that indicate a smaller $\mathbf{M_{max}}$ based on fault-dimension approaches. Such situations can lead to very large calculated static stress drops. Such considerations led two PSHA teams (DFS, RYA), in assessing $\mathbf{M_{max}}$, to rely only on approaches based on rupture length or rupture area. Only one team (SBK) explicitly provided a probability distribution for static stress drop (value [bars]/weight: 30/0.2, 35/0.5, 50/0.25, 100/0.05) and used the distribution in one approach to estimate $\mathbf{M_{max}}$ (CRWMS M&O 1998, Appendix E).

A value of static stress drop is calculated according to Equation 16 for each combination of rupture length, down-dip width, and $\mathbf{M_{max}}$ used in the PSHA. The radius of an equivalent circular rupture area is determined from the fault rupture length (L) and down-dip width (W) by:

$$a = \left(\frac{L \times W}{\pi} \right)^{0.5} \qquad \text{(Eq. 17)}$$

Next, the potential water table rise is computed using the calculated static stress drop and corresponding vertical extent of faulting ($W \times \sin(\textit{fault dip})$) using Equation 12. In this initial phase of the evaluation, neither the probability of each combination of rupture length, down-dip width, and $\mathbf{M_{max}}$ nor the probability of occurrence of an $\mathbf{M_{max}}$ earthquake are taken into account. Table 1 summarizes the results in terms of 25-m water table rise bins.

Given the approximately 187-m distance between the elevation of the water table (both currently and for future wetter climates) and the elevation of the lowest waste emplacement drift (SAR Section 1.3.1.1), most calculated values of water table rise have no flooding impact on the drift environment, regardless of their likelihood to occur or the conservatism of the model representation used to compute them. Of the 3,150 combinations evaluated, only 13 have a calculated water table rise greater than 175 m (Table 1).

Table 1. Summary of Water Table Rise Calculated Using the Bounding Kemeny and Cook Model for Combinations of Rupture Length, Down-dip Width, and Maximum Magnitude Interpreted in the PSHA

Water Table Rise (m)	Number of Rupture Length – Down-dip Width – Maximum M Combinations						
	AAR	ASM	DFS	RYA	SBK	SDO	Total
0 to 25	693	144	278	291	219	750	2,375
>25 to 50	35	45	0	120	72	95	367
>50 to 75	55	12	0	6	14	98	185
>75 to 100	27	12	0	0	9	75	123
>100 to 125	24	4	0	0	8	11	47
>125 to 150	18	3	0	0	1	1	23
>150 to 175	12	0	0	0	0	5	17
>175 to 200	5	0	0	0	0	0	5
>200 to 225	2	0	0	0	0	1	3
>225 to 250	1	0	0	0	0	1	2
> 250	1	1	0	0	0	1	3
Total	873	221	278	417	323	1,038	3,150

Source: Calculations based on the PSHA seismic source characterization

NOTE: Results are for combinations of rupture length, down-dip width, and $\mathbf{M_{max}}$ interpreted by the seismic source characterization teams and used in the PSHA, regardless of their assessed probability. Static stress drop is calculated using Equation 16 and water table rise is calculated using Equation 12. AAR, ASM, DFS, RYA, SBK, and SDO refer to the seismic source characterization teams who participated in the PSHA for Yucca Mountain.

In the next phase, the probabilities of the 13 combinations of rupture length, down-dip width, and $\mathbf{M_{max}}$ leading to calculated water table rise greater than 175 m are examined. The combined probability associated with a given combination of rupture dimensions and $\mathbf{M_{max}}$ depends on interpretations by the PSHA expert teams of the following:

- Probability that the fault source is active
- Probability of the logic tree branch leading to the combination
- Probability that $\mathbf{M_{max}}$ is the actual maximum magnitude
- Rate of occurrence of an earthquake with $\mathbf{M_{max}}$.

Table 2 summarizes the details of the seismic source characterizations for the 13 combinations. In general, large static stress drops, and thus large calculated values of water table rise, result from source characterizations that combine a large $\mathbf{M_{max}}$ with a short fault-rupture length and a short down-dip width. These combinations generally involve minor faults; a down-dip width constrained by a shallow extent to the seismogenic depth, a shallow detachment surface, or truncation by another fault at shallow depth; and an $\mathbf{M_{max}}$ distribution based in part on approaches (e.g., coseismic displacement, long-term slip rate) other than those tied to fault rupture dimension (e.g., length, area).

Table 2. Seismic Source Characterization Details for Combinations Giving Calculated Water Table Rise of Greater than 175 Meters

PSHA SSC Team[1]	Fault	Probability of Activity	M_{max}[2]	Rupture Length (km)	Dip (deg)	Down-dip Width (km)	Static Stress Drop (bars)	Calculated Water Table Rise (m)	Logic Tree Branch Probability	Annual Recurrence Rate[3]	Combined Annual Probability
AAR	Ghost Dance	0.1	6.4	2.0	70	4.8	3,671	198	7.61×10^{-4}	3.24×10^{-8}	3.94×10^{-13}
									3.26×10^{-4}	4.38×10^{-8}	
AAR	Ghost Dance	0.1	6.5	2.5	70	4.8	3,711	200	1.02×10^{-3}	1.8×10^{-8}	3.59×10^{-13}
									4.35×10^{-4}	3.95×10^{-8}	
AAR	Iron Ridge	1.0	6.9	6.0	60	5.2	3,515	190	2.54×10^{-3}	9.19×10^{-8}	1.69×10^{-10}
									1.09×10^{-3}	1.33×10^{-6}	
AAR	Midway Valley	0.1	6.7	4.0	70	4.8	3,658	198	2.54×10^{-3}	5.77×10^{-8}	5.06×10^{-12}
									1.09×10^{-3}	3.26×10^{-7}	
AAR	West Dune Wash #1	0.1	7.0	7.0	80	4.6	4,778	258	2.54×10^{-3}	8.58×10^{-9}	2.39×10^{-12}
									1.09×10^{-3}	1.97×10^{-7}	
AAR	West Dune Wash #1	0.1	7.0	7.0	80	7.1	2,463	207	8.64×10^{-3}	1.34×10^{-8}	1.27×10^{-11}
									3.70×10^{-3}	3.07×10^{-7}	
AAR	West Dune Wash #1	0.1	7.0	7.0	80	9.1	1,689	182	2.54×10^{-3}	1.72×10^{-8}	4.78×10^{-12}
									1.09×10^{-3}	3.95×10^{-7}	
AAR	West Dune Wash #2	0.1	6.6	3.0	80	4.6	4,278	231	2.49×10^{-2}	9.24×10^{-8}	5.83×10^{-11}
									1.07×10^{-2}	3.25×10^{-7}	
AAR	West Dune Wash #2	0.1	6.6	3.0	80	7.1	2,205	185	8.64×10^{-3}	1.44×10^{-7}	3.15×10^{-11}
									3.70×10^{-3}	5.06×10^{-7}	

Table 2. Seismic Source Characterization Details for Combinations Giving Calculated Water Table Rise of Greater than 175 Meters (continued)

PSHA SSC Team[1]	Fault	Probability of Activity	M_{max}[2]	Rupture Length (km)	Dip (deg)	Down-dip Width (km)	Static Stress Drop (bars)	Calculated Water Table Rise (m)	Logic Tree Branch Probability	Annual Recurrence Rate[3]	Combined Annual Probability
ASM	Iron Ridge	0.9	7.2	8.5	78	6.1	4,581	330	3.50×10^{-1}	2.15×10^{-8}	6.48×10^{-7}
									1.00×10^{-1}	1.27×10^{-6}	
									3.50×10^{-1}	1.38×10^{-5}	
									1.00×10^{-1}	1.38×10^{-5}	
									1.44×10^{-2}	1.84×10^{-8}	
									3.56×10^{-2}	6.62×10^{-8}	
									1.44×10^{-2}	1.11×10^{-5}	
									3.56×10^{-2}	1.66×10^{-5}	
SDO	Stagecoach Road	1.0	7.0	4.5	55	11.1	2,446	267	5.4×10^{-2}	1.78×10^{-5}	5.41×10^{-8}
									6.00×10^{-3}	1.80×10^{-5}	
SDO	Stagecoach Road	1.0	7.0	4.5	55	13.3	1,865	244	1.62×10^{-1}	1.78×10^{-5}	1.62×10^{-7}
									1.80×10^{-2}	1.80×10^{-5}	
SDO	Stagecoach Road	1.0	7.0	4.5	55	17.6	1229	212	5.40×10^{-2}	1.78×10^{-5}	5.41×10^{-8}
									6.00×10^{-3}	1.80×10^{-5}	

Source: Calculations based on the PSHA seismic source characterization

NOTES: SSC = seismic source characterization.

[1] AAR, ASM, and SDO refer to seismic source characterization teams who participated in the PSHA for Yucca Mountain (CRWMS M&O 1998, Section 4.3).

[2] $\mathbf{M_{max}}$ is the maximum moment magnitude. The probability of the $\mathbf{M_{max}}$ value for all combinations in this table is 0.1011.

[3] Multiple values represent alternative approaches to assessing annual recurrence rate. Recurrence rates are calculated from PSHA seismic source characterization data using relations presented in CRWMS M&O 1998, Section 4.1.4.

All interpreted combinations by the AAR team resulting in a calculated water table rise greater than 175 m have combined annual probabilities (i.e., probability of activity × $\mathbf{M_{max}}$ probability × sum of [logic tree branch probability × associated annual recurrence rate]) of about 10^{-10} or less. Combined annual probabilities for the ASM and SDO combinations are between 7×10^{-7} and 5×10^{-8} and do not fall below the 10^{-8} threshold for consideration in the total system performance assessment. Nevertheless, given the identified sources of overestimation (Section 1.2.1) in the bounding Kemeny and Cook representation used to calculate water table rise in this analysis, these results strongly support the consistency of the screening evaluation for FEP 1.2.10.01.0A, *Hydrologic Response to Seismic Activity*, with the seismic source characterization of the PSHA.

1.2.3 Estimates of Potential Water Table Rise Based on PSHA Fault Displacement Hazard Results

Based on the results of the PSHA, an alternative approach to assessing the potential for water table rise at Yucca Mountain is to use fault displacement hazard results. Of the nine demonstration locations at the site for which fault displacement hazard was determined, the largest hazard occurred for a location on the Solitario Canyon fault. Extrapolation of that displacement hazard to a 10^{-8} mean annual probability of exceedance yields a fault displacement of 13 m (SAR Table 2.2-15). This value is taken as average displacement over the rupture area (U in cm) of a block-bounding fault (e.g., Solitario Canyon fault or Paintbrush Canyon fault). While the average displacement at or near the surface may be less than the average over the entire rupture area, this limitation is offset because the fault displacement hazard result contains contributions from both primary and secondary faulting.

To assess the implications of a 13-m fault displacement for water table rise, the displacement is used along with interpretations of rupture length and down-dip width from the PSHA to calculate static stress drop. Kanamori and Anderson (1975, Figure 1) give:

$$\Delta\sigma_{static} = \frac{7\pi}{16}\mu\frac{U}{a} \qquad \text{(Eq. 18)}$$

in which μ is the shear modulus (taken as 3×10^{11} dyne/cm^2). As in Section 1.2.2, the rupture area for an interpreted rupture length and down-dip width is used to determine the radius of an equivalent circular area. Then, static stress drop is calculated from Equation 18 and used in Equation 12 with the associated vertical extent of faulting to compute a water table rise. This process is carried out for each combination of rupture length and down-dip width for a given fault interpretation. Then, a weighted water table rise is calculated for that fault interpretation using the logic tree branch probabilities as the weights. Because a given fault may be the subject of alternative interpretations (e.g., acting independently or linked with other faults) the sum of the logic tree branch probabilities for a given interpretation is often less than 1.0. Thus, the water table rise for a given interpretation is normalized to the sum of branch probabilities for that interpretation. The calculation was carried out for the Solitario Canyon fault and the Paintbrush Canyon fault, and for fault combinations including them, using the rupture lengths and down-dip widths interpreted by the PSHA teams. Results are summarized in Table 3.

The results below update the inference in *Features, Events, and Processes for the Total System Performance Assessment: Analyses* (SNL 2008, FEP 1.2.10.01.0A) associating a water table rise of no more than 50 m with 13 m of slip during an earthquake on the Solitario Canyon fault. Using the bounding Kemeny and Cook (1992) representation and seismic source characterization interpretations from the PSHA, average water table rise for a 13-m slip event ranges from 30 to 122 m.

Table 3. Summary of Calculated Water Table Rise Using the Bounding Kemeny and Cook (1992) Model of an Earthquake Displacement with a 10^{-8} Mean Annual Probability of Being Exceeded

PSHA SSC Team	Fault	Average Weighted Static Stress Drop (bars)	Range of Water Table Rise (m)	Average Weighted Water Table Rise (m)[1]	Interpretation Weight[2]
AAR	Solitario Canyon	609	56 to 109	98	0.222
AAR	Stagecoach Road – Paintbrush Canyon	573	50 to 101	91	0.155
AAR	Paintbrush Canyon	688	62 to 114	107	0.067
AAR	Single (Coalesced, Pattern 1)	373	25 to 35	30	0.009
AAR	Single West Side (Coalesced, Pattern 3)	429	36 to 70	58	0.171
AAR	Single Yucca Mountain System (Coalesced, Pattern 2)	431	28 to 40	35	0.015
AAR	West Side 1 (Coalesced, Pattern 4)	643	56 to 103	93	0.583
ASM	Solitario Canyon	616	70 to 102	75	0.95
ASM	Stagecoach Road – Paintbrush Canyon	494	65 to 92	75	0.95
DFS	Solitario Canyon	646	50 to 83	74	0.950
DFS	Stagecoach Road – Paintbrush Canyon	521	31 to 87	73	0.950
DFS	Distributed Faulting Scenario A	317	32 to 42	39	0.010
DFS	Distributed Faulting Scenario B	285	29 to 38	35	0.030
DFS	Distributed Faulting Scenario C	263	26 to 35	32	0.010
RYA	Paintbrush Canyon – Stagecoach Road – Bow Ridge (Coalescing, 2 and 3 faults)	567	62 to 189	100	0.880
RYA	Solitario Canyon – Iron Ridge	596	80 to 205	105	0.390
RYA	Single Coalescing	463	74 to 100	86	0.120
RYA	West Side (Coalescing, 2 faults)	543	72 to 177	96	0.490

Table 3. Summary of Calculated Water Table Rise Using the Bounding Kemeny and Cook (1992) Model of an Earthquake Displacement with a 10^{-8} Mean Annual Probability of Being Exceeded (continued)

PSHA SSC Team	Fault	Average Weighted Static Stress Drop (bars)	Range of Water Table Rise (m)	Average Weighted Water Table Rise (m)[1]	Interpretation Weight[2]
SBK	Paintbrush Canyon	677	94 to 131	114	0.500
SBK	Paintbrush Canyon – Stagecoach Road	489	68 to 95	82	0.400
SBK	Solitario Canyon	613	65 to 107	85	0.500
SBK	Solitario Canyon – Iron Ridge	613	65 to 107	85	0.400
SBK	Coalesced	501	53 to 87	69	0.090
SBK	Detachment	422	29 to 58	46	0.010
SDO	North Paintbrush Canyon	692	82 to 185	115	0.407
SDO	North Paintbrush Canyon – Bow Ridge	654	80 to 173	109	0.009
SDO	Paintbrush Canyon	557	70 to 130	93	0.096
SDO	Paintbrush Canyon – Bow Ridge	557	70 to 130	93	0.009
SDO	Paintbrush Canyon – Stagecoach Road	452	61 to 104	75	0.096
SDO	Paintbrush Canyon – Stagecoach Road – Bow Ridge	452	61 to 104	75	0.009
SDO	Solitario Canyon	586	67 to 98	83	0.575
SDO	Solitario Canyon – South Windy Wash	514	62 to 83	73	0.125
SDO	South Paintbrush Canyon	720	107 to 150	120	0.236
SDO	South Paintbrush Canyon – Bow Ridge	644	90 to 136	107	0.074
SDO	South Paintbrush Canyon – Stagecoach Road	542	80 to 115	90	0.042
SDO	Stagecoach Road	917	90 to 185	122	0.500
SDO	Stagecoach Road – Solitario Canyon	478	62 to 100	79	0.125

Source: Calculations based on the PSHA seismic source characterization and fault displacement hazard results. .

NOTES: [1]To compute the average water table rise, values are weighted according to their logic tree branch probabilities times the maximum magnitude probability and normalized to the total weight that the given interpretation is active.

[2]Interpretation weight is the probability that a given fault configuration (i.e., acting independently, linked with other faults) represents the tectonic conditions at Yucca Mountain. The interpretation weight is the sum of the underlying logic tree branch probabilities when the fault configuration is active.

Calculated values of average weighted water table rise based on a fault displacement of 13 m and using the fault source characterization results from the PSHA expert teams are 122 m or less. Thus, for a displacement with a nominal 10^{-8} mean annual probability of being exceeded, a bounding estimate of water table rise still leaves a distance of 65 m or more between the

elevation of the water table and the elevation of the lowest waste emplacement drift. Note also that for most fault interpretations evaluated, the logic tree branch probability is significantly less than 1. Consequently, exclusion of FEP 1.2.10.01.0A, *Hydrologic Response to Seismic Activity*, from the Total System Performance Assessment is consistent with the seismic source characterization interpretations and the fault displacement hazard results of the PSHA.

1.2.4 Implications for Previous RAI Responses

In the responses to RAI 3.2.2.1.2.1-2-019, its Supplemental Question 6, and RAI 3.2.2.1.2.1-5-001, water table rise was evaluated using a modified version of the Kemeny and Cook (1992, Equation 6.1) representation of the poroelastic response to an earthquake. Estimates determined from the bounding Kemeny and Cook (1992) representation were modified by adjusting them upward based on the assumption that, for a 100-bar static stress drop and 10-km vertical extent of faulting, a 50-m rise in water table resulted. The Kemeny and Cook (1992) representation gives a 12-m water table rise for these inputs.

As the analysis of earthquake-induced water table rise has been further developed in this response to include consideration of extreme static stress drops, the modification that was earlier added to the Kemeny and Cook (1992) representation is dropped. Even without this additional conservatism, the output of the Kemeny and Cook (1992) representation was intended to be bounding (see Section 1.2.1). Here, results presented in previous responses are updated to use the Kemeny and Cook (1992) representation without modification.

Previous responses are also revised to reflect an updated evaluation of the empirical relation between median point-source stress drop and median static stress drop (see the response to Supplemental Question 7). This updated evaluation finds they have approximately the same value.

Update to Response to RAI 3.2.2.1.2.1-2-019

In the original response to RAI 3.2.2.1.2.1-2-019, water table rise was estimated for an earthquake on the Solitario Canyon fault, consistent with an approach used to condition extreme ground motion for Yucca Mountain. The earthquake was assumed to have a point-source stress drop whose probability, when combined with a 3×10^{-5} annual rate of occurrence of maximum magnitude events, led to a 10^{-8} annual probability of exceedance. In the previous response, the probability of exceedance for the point-source stress drop was determined from a lognormal distribution with a median of 60 bars and a lognormal standard deviation of 0.5. Updated results based on a more extensive database of earthquake strong ground motion records give a revised lognormal distribution for point-source stress drop with a median of 28.8 bars and a lognormal standard deviation of 0.59 (see response to Supplemental Question 7). These results indicate that median point-source stress drop and median static stress drop are about equal (see response to Supplemental Question 7). For this updated lognormal distribution, a point-source stress drop of about 215 bars, conditional on a large earthquake occurring on the Solitario Canyon fault, has a probability of exceedance of about 10^{-8} or less. Previously a value of 330 bars was determined.

Taking this point-source stress drop as equivalent to a static stress drop of 215 bars, and using a vertical extent of faulting of 10 km, the bounding Kemeny and Cook (1992) representation (Equation 12) yields an estimated water table rise of 26 m. This value compares to a value of 80 m provided in the original response, which was based on the previously determined relation between point-source stress drop and static stress drop and the modified version of the bounding Kemeny and Cook (1992) representation.

Update to Response to RAI 3.2.2.1.2.1-2-019, Supplemental Question 6

In response to Supplemental Question 6, the analysis provided in the original response was expanded to consider the effect of other faults in the vicinity of Yucca Mountain and the effects of earthquakes of smaller magnitude. The effect of faults within about 20 km of the site was incorporated by substituting their combined annual rate of occurrence for the rate based only on the Solitario Canyon fault. This calculation resulted in an estimated water table rise of 100 m using the modified version of the bounding Kemeny and Cook (1992) representation. Using the updated lognormal distribution for point-source stress drop, taking static stress drop as equal to point-source stress drop, and using Equation 12, a revised calculation gives 32 m for a 270 bar static stress drop and a 10-km vertical extent of faulting.

In examining the effect of smaller magnitude earthquakes in the response to Supplemental Question 6, the down-dip width (and thus vertical extent) of faulting was explicitly incorporated rather than assuming a value of 10 km for all cases. Down-dip width was estimated empirically as a function of magnitude. Water table rise ranged from about 55 to 115 m for magnitudes from 5.50 to 6.75. Table 4 provides a revision of Table 1 from the response to Supplemental Question 6. Table 4 reflects the updated information presented in this response and in the response to Supplemental Question 7.

Table 4. Combined Impact of Change in Static Stress Drop and Change in Vertical Extent of Fault Rupture (Updated)

Moment Magnitude	Annual Frequency[a]	Point-Source Stress Drop with a Probability of Exceedance of 10^{-8} (bars)[b]	Static Stress Drop with a Probability of Exceedance of 10^{-8} (bars)[c]	Vertical Extent of Faulting (km)[d]	Water Table Rise (m)[e]
5.5	4.0×10^{-4}	320	320	5	19
6.0	1.3×10^{-4}	270	270	8	26
6.5	5.0×10^{-5}	240	240	12	35
6.75	2.0×10^{-5}	210	210	14	35

[a] Annual frequency is determined from CRWMS M&O 1998, Figure 4-74.

[b] Point-source stress drop with a probability of exceedance of 10^{-8} is determined using a lognormal distribution with a median of 28.8 bars and a lognormal standard deviation of 0.59.

[c] Static stress drop with a probability of exceedance of 10^{-8} is taken as equal to point-source stress drop.

[d] Vertical extent of faulting is computed using the Wells and Coppersmith 1994, Table 2A, empirical relation between the logarithm of rupture width (RW) in kilometers and moment magnitude (M). The relation based on normal faulting events is used: log (RW) =−1.14 + 0.35 M. A fault dip of 60 degrees is used to comp ute vertical extent of faulting from down-dip rupture width.

[e] Water table rise is computed using the Kemeny and Cook 1992 representation (Equation 12).

Update to Response to RAI 3.2.2.1.2.1-5-001

In the discussion of water table rise due to seismic activity included in the response to RAI 3.2.2.1.2.1-5-001, the same results were provided as in the response to RAI 3.2.2.1.2.1-2-019, Supplemental Question 6. Taking into account local faults and considering earthquakes with moment magnitude from 5.5 to 6.75, water table rise was bounded at about 115 m for a moment magnitude of 6.75 with a static stress drop of 155 bars. As shown in Table 4, updated results for a moment magnitude 6.75 event are characterized by a point-source stress drop of 210 bars, a static stress drop taken as equal to the point-source stress drop (210 bars), a vertical extent of faulting of 14 km, and a bounding water table rise of 35 m. Based on the this updated analysis, the evaluation of water table rise consistent with the results of the PSHA, and the documentation of the overestimation of water table rise by the Kemeny and Cook (1992) model, the conclusion of the screening evaluation to exclude FEP 1.2.10.01.0A, *Hydrologic Response to Seismic Activity*, is confirmed.

1.3 SUMMARY

Static stress drop, which is a key input to the regional stress change model for estimating a bound to water table rise (Kemeny and Cook 1992), is weakly correlated to strong ground motion (Section 1.1, Response to Supplemental Question 7). Thus, it is not possible to estimate the static stress drop associated with a value of strong ground motion that, based on the PSHA, has a 10^{-8} mean annual probability of exceedance (e.g., horizontal PGV for the repository waste emplacement level of 4.07 m/s). Rather, consistency of the screening evaluation for FEP 1.2.10.01.0A, *Hydrologic Response to Seismic Activity*, with the results of the PSHA is demonstrated by calculating static stress drop based on seismic source characterization and fault displacement hazard results and then using the bounding Kemeny and Cook (1992) model to estimate water table rise.

Two approaches based on the PSHA results are investigated. One calculates static stress drop for combinations of maximum magnitude, fault rupture length, and down-dip width interpreted by the PSHA experts for local faults in the vicinity of Yucca Mountain. Following this approach, most combinations lead to bounding water table rise values less than 187 m, the approximate distance between the water table (both current and for future wetter climates) and the lowest elevation waste emplacement drift. When the assumptions underlying the Kemeny and Cook (1992) model are considered in light of the current understanding of seismic-induced hydrologic responses, it is concluded that estimates of bounding water table rise based on the model significantly overestimate realistic values. Thus, even though a small number of PSHA seismic source characterization combinations lead to bounding water table rise greater than 187 m, the overall conclusion, taking into account the nature of the model, is that the screening evaluation to exclude FEP 1.2.10.01.0A, *Hydrologic Response to Seismic Activity*, is strongly supported.

A second approach calculates static stress drop for fault interpretations involving the Solitario Canyon and Paintbrush Canyon faults using combinations of rupture length and down-dip width from the PSHA, along with a fault displacement value (13 m) that has a 10^{-8} mean annual probability of being exceeded for the Solitario Canyon fault. Following this approach, the average weighted water table rise using the bounding Kemeny and Cook (1992) model ranges

from 30 to 122 m for the faults evaluated. This range characterizes static stress drops with a 10^{-8} mean annual probability of being exceeded based on the PSHA fault displacement hazard results. All of the faults result in an estimated water table rise that is 65 m or more below the lowest elevation of the repository waste emplacement drifts. Thus, this approach confirms the screening evaluation to exclude FEP 1.2.10.01.0A, *Hydrologic Response to Seismic Activity*.

2. COMMITMENTS TO NRC

None.

3. DESCRIPTION OF PROPOSED LA CHANGE

None.

4. REFERENCES

Abrahamson, N. and Silva, W. 2008. "Summary of the Abrahamson & Silva NGA Ground-Motion Relations." *Earthquake Spectra, 24*, (1), 67-97. Oakland, California: Earthquake Engineering Research Institute.

Aki, K. and Richards, P.G. 1980. Quantitative Seismology, Theory and Methods. Two volumes. San Francisco, California: W.H. Freeman and Company.

Belcher, W.R. 2004. *Death Valley Regional Ground-Water Flow System, Nevada and California - Hydrogeologic Framework and Transient Ground-Water Flow Model.* Scientific Investigations Report 2004-5205. Reston, Virginia: U.S. Geological Survey. ACC: MOL.20050323.0070[a].

Brune, J.N. 1970. "Tectonic Stress and the Spectra of Seismic Shear Waves from Earthquakes." *Journal of Geophysical Research, 75*, (26), 4997-5009. Washington, D.C.: American Geophysical Union.

Brune, J.N. 1971. "Tectonic Stress and the Spectra of Seismic Shear Waves from Earthquakes Correction." *Journal of Geophysical Research, 76,* (20), 5002. Washington, D.C.: American Geophysical Union.

BSC (Bechtel SAIC Company) 2004. *Water-Level Data Analysis for the Saturated Zone Site-Scale Flow and Transport Model.* ANL-NBS-HS-000034 REV 02. Las Vegas, Nevada: Bechtel SAIC Company. ACC: DOC.20041012.0002

Carrigan, C.R.; King, G.C.P.; Barr, G.E.; and Bixler, N.E. 1991. "Potential for Water-Table Excursions Induced by Seismic Events at Yucca Mountain, Nevada." *Geology, 19*, (12), 1157-1160. Boulder, Colorado: Geological Society of America.

Cook, N.G.W. and Kemeny, J.M. 1991. "A Mechanical Estimate for Water Level Change Due to a Normal Faulting Earthquake." *Eos, Transactions (Supplement), 72,* (17), 116. Washington, D.C.: American Geophysical Union.

CRWMS M&O 1998. *Probabilistic Seismic Hazard Analyses for Fault Displacement and Vibratory Ground Motion at Yucca Mountain, Nevada*. Milestone SP32IM3, September 23, 1998. Three volumes. Las Vegas, Nevada: CRWMS M&O. ACC: MOL.19981207.0393.

Cutillo, P.A. and Ge, S. 2006. "Analysis of Strain-Induced Ground-Water Fluctuations at Devils Hole, Nevada." *Geofluids, 6,* 319-333. Malden, Massachusetts: Blackwell Publishing.

Grecksch, G, Roth, F., and Kuempel, H-J 1999. "Coseismic Well-level Changes due to the 1992 Roermond Earthquake Compared to Static Deformation of Half-space Solutions." *Geophysical Journal International, 138*, (2), 470 – 478. Oxford, England: Blackwell Publishing.

Hanks, T.C. and Kanamori, H. 1979. "A Moment Magnitude Scale." *Journal of Geophysical Research, 84,* (B5), 2348-2350. Washington, D.C.: American Geophysical Union.

Jonsson, S.; Segall, P.; Pedersen, R.; and Bjornsson, G. 2003. "Post-Earthquake Ground Movements Correlated to Pore-Pressure Transients." *Nature, 424,* 179-183. London, England: Nature Publishing Group.

Kanamori, H. and Anderson, D.L. 1975. "Theoretical Basis of Some Empirical Relations in Seismology." *Bulletin of the Seismological Society of America, 65*, (5), 1073-1095. El Cerrito, California: Seismological Society of America.

Kemeny, J. and Cook, N. 1990. "Rock Mechanics and Crustal Stress." Section 5 of *Demonstration of a Risk-Based Approach to High-Level Waste Repository Evaluation*. McGuire, R.K., ed. EPRI NP-7057. Palo Alto, California: Electric Power Research Institute.

Kemeny, J.M. and Cook, N.G.W. 1992. "Water Table Change Due to a Normal Faulting Earthquake." Section 6 of *Demonstration of a Risk-Based Approach to High-Level Waste Repository Evaluation: Phase 2*. EPRI TR-100384. Palo Alto, California: Electric Power Research Institute.

King, C.-Y. and Igarashi, G. 2002. Earthquake related hydrological and geochemical changes, *International Handbook of Earthquake and Engineering Seismology,* Part A, W.H.K. Lee et al., eds, pp 637-645, Academic Press, Amsterdam.

Koizumi, N.; Matsumoto. N.; Fujita, A.; Sato, T.; and Kitagawa, Y. 2005. "Evaluation of Groundwater Changes Caused by the 2003 Tokachi-oki Earthquake (M8.0)." *EOS Transactions (Supplement), 86*, (52), Abstract H41F-0464. Washington, D.C.: American Geophysical Union.

Manga, M. and Wang, C.-Y. 2007. *Earthquake Hydrology,* Treatise on Geophysics, G. Schubert editor, volume 4, 293-320.

National Research Council. 1992. *Ground Water at Yucca Mountain, How High Can It Rise? Final Report of the Panel on Coupled Hydrologic/Tectonic/Hydrothermal Systems at Yucca Mountain*. Washington, D.C.: National Academy Press.

O'Brien, G.M. 1993. *Earthquake-Induced Water-Level Fluctuations at Yucca Mountain, Nevada, June 1992*. Open-File Report 93-73. Denver, Colorado: U.S. Geological Survey. ACC: NNA.19930326.0022.

Paces, J.B.; Neymark, L.A.; Marshall, B.D.; Whelan, J.F.; and Peterman, Z.E. 2001. *Ages and Origins of Calcite and Opal in the Exploratory Studies Facility Tunnel, Yucca Mountain, Nevada*. Water-Resources Investigations Report 01-4049. Denver, Colorado: U.S. Geological Survey. ACC: MOL.20020115.0207[b].

Quilty, E. and Roeloffs, E. 1994. "Water Level Changes in Response to the December 20, 1994 M4.7 Earthquake near Parkfield, California." *Bulletin of the Seismological Society of America, 87*, 310-317. El Cerrito, California: Seismological Society of America.

Roeloffs, E. 1996. "Poroelastic Techniques in the Study of Earthquake-Related Hydrologic Phenomena." *Advances in Geophysics, 37,* 135-195. New York, New York: Academic Press.

Roeloffs, E.A. 1998. "Persistent Water Level Changes in a Well near Parkfield California, due to Local and Distant Earthquakes." *Journal of Geophysical Research, 103,* (B1), 869-889. Washington, D.C.: American Geophysical Union.

Sato, T.; Matsumoto, N.; Kitagawa, Y.; Koizumi, N; Takahashi, M.; Kuwahara, Y. 2003. "Changes in Groundwater Level Associated with the 2003 Tokachi-oki Earthquake." *Earth Planets and Space, 56,* (3), 395-400. Tokyo, Japan: Terra Scientific Publishing Company.

Silva, W.J.; Abrahamson, N.; Toro, G.; and Costantino, C. 1996. *Description and Validation of the Stochastic Ground Motion Model*. PE&A 94PJ20. El Cerrito, California: Pacific Engineering and Analysis.

SNL (Sandia National Laboratories) 2008. *Features, Events, and Processes for the Total System Performance Assessment: Analyses*. ANL-WIS-MD-000027 REV 00. Las Vegas, Nevada: Sandia National Laboratories. ACC: DOC.20080307.0003; DOC.20080407.0009; LLR.20080522.0166.

Wang, H.E. 2000. *Theory of Linear Poroelasticity with Applications to Geomechanics and Hydrogeology*, Princeton, N.J., Princeton University Press.

Whelan, J.F.; Neymark, L.A.; Moscati, R.J.; Marshall, B.D.; and Roedder, E. 2008. "Thermal History of the Unsaturated Zone at Yucca Mountain, Nevada, USA." *Applied Geochemistry, 23,* 1041-1075. New York, New York: Elsevier.

Wilson, N.S.F.; Cline, J.S.; and Amelin, Y.V. 2003. "Origin, Timing, and Temperature of Secondary Calcite–Silica Mineral Formation at Yucca Mountain, Nevada." *Geochimica et Cosmochimica Acta, 67*, (6), 1145-1176. New York, New York: Pergamon.

NOTES: [a]Provided as an enclosure to letter from Williams to Sulima, dtd 6/5/09, "Yucca Mountain – Supplemental Response to Request for Additional Information – Safety Evaluation Report Volume 3, Postclosure Chapter 2.2.1.2.1 (Scenario Analysis), Second Set."

[b]Provided as an enclosure to letter from Williams to Sulima, dtd 7/20/09, "Yucca Mountain – Request for Additional Information – Safety Evaluation Report, Volume 3 — Postclosure Chapter 2.2.1.3.6, Set 2 – Flow Paths in the Unsaturated Zone – (Department of Energy's Safety Analysis Report Sections 2.3.2, 2.3.3, and 2.3.5)."

RAI Volume 3, Chapter 2.2.1.2.1, Second Set, Number 19, Supplemental Question 7:

> Clarify the basis for the statement that residual static stress drop following an earthquake is approximately half the point source stress drop. How does this definition relate to the one given in paragraph 1 on page 9 of the RAI response which states that static stress drop is simply an expression involving slip or displacement on the fault during rupture?

1. SUPPLEMENTAL RESPONSE

The screening evaluation for FEP 1.2.10.01.0A, *Hydrologic Response to Seismic Activity*, relies in part on a simple, bounding representation of the poroelastic response of the earth's crust to an earthquake (Kemeny and Cook 1990, 1992). In this representation, water table rise is related to static stress drop[1] and the vertical extent of faulting. In the response to RAI 3.2.2.1.2.1-2-019, consistency of the screening evaluation with seismic analyses to develop ground motion inputs for design and performance assessment was addressed. Specifically, consistency with an approach used to condition extreme ground motion such that it is consistent with the geologic setting at Yucca Mountain was examined. This conditioning approach involves developing a probability distribution for extreme point-source stress drop. To relate this parameter to static stress drop, used in the screening evaluation, required the development of a relation between the two. The relation between median point-source stress drop and median static stress drop was, therefore, developed using an empirical basis (see the response to RAI 3.2.2.1.2.1-2-019, Section 1.2.3).

A theoretical development shows that static stress drop and stress parameter (point-source stress drop) have an equivalent form, although static stress drop is related to the static aspects of the earthquake, while stress parameter is related to the dynamics of rupture. The empirical relation between median static stress drop and median stress parameter has been updated on the basis of the earthquake database compiled for the Next Generation of Ground-Motion Attenuation Models (NGA) project (Power et al. 2008) and other recent events. This analysis shows that, although theoretically linked, there is a lack of correlation between static stress drop and stress parameter on an individual earthquake basis. The results of the updated analysis show that median static stress drop is about equal to median stress parameter (point-source stress drop) and not half its value as was stated in the responses to RAI 3.2.2.1.2.1-2-019 and Supplemental Questions 1 and 6, which were based on previous analyses. Implications of the updated result with respect to previous responses to RAI 3.2.2.1.2.1-2-019, its Supplemental Questions, and RAI 3.2.2.1.2.1-5-001 are discussed in Section 1.2.4 of the response to Supplemental Question 5. The updated result does not alter the conclusion presented in earlier responses that the screening evaluation of FEP 1.2.10.01.0A is consistent with seismic analyses described in the SAR.

[1] Static stress drop is the difference between the average shear stress on the fault before and after an earthquake and is the same quantity as residual static stress drop.

1.1 STATIC STRESS DROP EQUIVALENCE TO STRESS PARAMETER

As noted in Section 1.1 of the response to Supplemental Question 5 and discussed in more detail in Section 1.2 of this response, static stress drop ($\Delta\sigma_{static}$) is weakly correlated to the stress parameter ($\Delta\sigma_{SP}$) and the overall level of strong ground motions. The static stress drop for a circular rupture is given by (Brune 1970; Kanamori and Anderson 1975):

$$\Delta\sigma_{static} = \frac{7}{16}\frac{M_0}{a^3} \qquad \text{(Eq. 1)}$$

in which M_0 is the earthquake moment and a the radius of the circular rupture. For a rectangular rupture expressed in terms of length (L) and width (W), an equivalent radius can be expressed as:

$$a^2 = \frac{L \cdot W}{\pi}$$

The linkage between the static stress drop and the stress parameter is through the effects of source finiteness. The omega-squared (frequency-squared) source model is a widely accepted way to describe the frequency dependence of earthquake ground motion (Aki and Richards 1980). For a rectangular rupture, the frequency-squared dependence of the far field source model is due to the combination of a finite rupture length and associated duration of rupture, as well as a finite time for the slip to attain its maximum value along the rupture (rise time). For the circular rupture model of Brune, the frequency-squared dependence is due to the rupture finiteness alone; slip being theoretically instantaneous at all points on the rupture surface (Brune 1970, 1971). Since the rise time is much shorter than the rupture duration (Heaton 1990), it is neglected in this model and the characteristic source duration (τ) is simply the time required to propagate from the center of the circular rupture to the edge:

$$\tau = \frac{a}{V_R} \qquad \text{(Eq. 2)}$$

in which $\mathbf{V_R}$ is the rupture velocity and a the source radius, which can be replaced by L for length in a rectangular rupture. This characteristic duration gives rise to the corner frequency (f_C) in the omega-squared model:

$$f_C \propto \frac{1}{\tau} \propto \frac{V_R}{L} \qquad \text{(Eq. 3)}$$

The static stress drop for a general source is given by:

$$\Delta\sigma_{static} = C\,\mu\,\frac{\bar{u}}{L} \qquad \text{(Eq. 4)}$$

in which C is a geometric constant (7/16 for a circular rupture), μ is the shear modulus, and $\left(\frac{\bar{u}}{L}\right)$ is the strain drop (average slip $(\bar{u})$ over the characteristic dimension of the rupture (L)). Substituting the definition of moment:

$$M_0 = \mu\ \bar{u}\ L^2 \qquad \text{(Eq. 5)}$$

in which $\left(L^2\right)$ is a characteristic rupture area, into Equation 4 results in:

$$\Delta\sigma_{static} = C\ \frac{M_0}{L^3}, \qquad \text{(Eq. 6)}$$

and from Equation 3:

$$\Delta\sigma_{static} = C\ M_0\left(\frac{f_C}{V_R}\right)^3. \qquad \text{(Eq. 7)}$$

Static stress drop, therefore, shows the same functional dependence on M_0 and f_C as does Equation 1 of the response to Supplemental Question 5 for the stress parameter:

$$\Delta\sigma_{SP} = 8.44\, M_0\left(\frac{f_C}{\beta}\right)^3 \qquad \text{(Eq. 8)}$$

and reduces to Equation 1 of Supplemental Question 5 for a circular rupture, providing the theoretical linkage between $\Delta\sigma_{static}$ and $\Delta\sigma_{SP}$.

1.2 EMPIRICAL ANALYSES OF STATIC STRESS DROPS AND STRESS PARAMETERS

Conditional on magnitude, distance, and site condition, empirical analyses of strong ground motions have shown a significant dependence of spectral levels on source mechanism (Abrahamson and Shedlock 1997) and depth to the top of rupture (Power et al. 2008). Since the stress parameter is sensitive to spectral levels over a wide frequency range that increases with magnitude, it captures such dependencies in a predictable manner.

For static stress drop, increased values that may result in larger forces to accelerate the rupture with consequent potential impacts on slip and possibly rupture velocity are not reflected in observed increased ground motion spectral levels. To examine the empirical relationship that exists between static stress drop and stress parameter, as well as their dependence on magnitude, source mechanism, and depth to top of rupture, a suite of analyses was performed on a subset of the earthquakes in the NGA strong motion data set (Chiou et al. 2008), as well as on NGA ground motion prediction equations (GMPEs) (Power et al. 2008).

In the NGA database, static stress drop is calculated for the 63 earthquakes for which a finite fault model (finite rupture model) is available. Assuming a circular rupture, static stress drop is determined from the moment (M_0), which is based on magnitude, and rupture area. If available, finite rupture models derived from analyses of strong ground motion are used as the basis for rupture area. For earthquakes without finite rupture models based on strong motion data, rupture area estimates were primarily based on aftershock locations within about 24 hours of the mainshock (Wells and Coppersmith 1994). The finite fault models went through several iterations of reviews including by an NGA Working Group and by the NGA GMPE developers (Chiou et al. 2008, p. 34). Subsequent to development of the NGA database, data for five additional events (Table 1, EQIDs 176 to 180) have been processed in a similar manner, including development of finite fault models. For the 68 earthquakes with finite fault models, the database also includes an estimate of the depth from the ground surface to the top of the rupture.

Rupture areas provided in the NGA database, and for the five additional earthquakes, reflect consistent review of their underlying bases. Still, considerable uncertainty exists in the appropriate rupture area for an earthquake. For the same earthquake, different source and wave propagation models result in different slip models and, consequently, different rupture dimensions. In using aftershock locations, it is always somewhat arbitrary to develop an outline of locations to define a rupture area. These inherent uncertainties likely give rise to the large aleatory variability associated with static stress drops. The variability of static stress drop is significantly greater than that of the stress parameter, which is based on high-frequency spectral levels.

Treating static stress drop as log normally distributed, a median and lognormal standard deviation (σ_{ln}) of 30.6 bars and 0.86, respectively, were determined from the database (Table 2). In computing these values, aftershocks were not included (e.g., Chi-chi, Taiwan, Table 1, EQIDs 171 to 175) to avoid any potential bias from such events. Also, the Cape Mendocino earthquake was not included due to ambiguity about whether it is a crustal or subduction zone source. Thus a total of 62 earthquakes were used in the analysis. For the static stress drops, the median value of 30.6 bars is very close to the approximately 30-bar value that is consistent with the Wells and Coppersmith (1994) empirical relation between magnitude (**M**) and rupture area (see the response to RAI 3.2.2.1.2.1-2-019).

When plotted as a function of magnitude (Figure 1) and depth to top-of-rupture (Figure 2), it is apparent that static stress drop is not correlated with these parameters. These figures also demonstrate visually the large aleatory variability of the dataset.

Stress parameter estimates were performed for 29 of the 68 earthquakes in the database for which finite rupture models are available (Table 1). Stress parameters are estimated from inversions of the Fourier amplitude spectra of acceleration computed with recordings of the windowed shear-wave arrivals. The approach is described and illustrated in EPRI (1993) and Silva et al. (1996). It accommodates crustal as well as shallow site amplification for rock (Geomatrix A and B) and soil (Geomatrix C and D) sites (Silva et al. 1996), potential nonlinear effects in spectral damping through site-specific kappa determinations, and crustal damping through determination of region specific Q(f) models (Silva et al. 1996). Excluding aftershocks

again, stress parameter statistics based on 24 earthquakes are summarized in Table 2. The median stress parameter is 28.9 bars and the aleatory variability is 0.59 (σ_{ln}).

The median value of 28.9 is close to the median static stress drop value of 30.6 bars, but the aleatory variability is significantly lower for stress parameter; 0.59 compared to 0.86 for static stress drop. To ensure the subset of 24 earthquakes used for the stress parameter calculation does not affect the estimate of median static stress drop, median static stress drop and its lognormal standard deviation (σ_{ln}) were computed for the same 24 earthquakes. For the subset, the median estimate of static stress drop was reduced slightly from 30.6 bars to 26.1 bars, about 15%, while the aleatory variability increased slightly from 0.86 to 0.87 (σ_{ln}). Given this favorable agreement between the two sets of values, it is concluded that the sample subset of 24 events reflects the same distribution as the entire sample of 62 events.

A plot of static stress drop versus stress parameter for individual earthquakes (Figure 3) shows the lack of correlation between the two values. The correlation coefficient based on all 24 earthquakes is 0.0 (Table 2). When the earthquakes are categorized according to whether they are dominated by shallow or deep slip, correlation coefficients of -0.1 and -0.6 are obtained, respectively.

The change in the relation between median estimates of static stress drop and stress parameter, relative to values presented in the original response to RAI 3.2.2.1.2.1-2-019 is an artifact of the distributions of magnitude, source mechanism, and depth of slip for the earthquakes analyzed, all of which affect the stress parameter, likely in a correlated manner. The factor-of-two difference in the original response (static stress drop of about 30 bars; stress parameter of about 60 bars) was based on analyses of stress parameters (Silva et al. 1996; Atkinson and Silva 1997) that included fewer large magnitude earthquakes than the current analysis. The stress parameter depends strongly on both magnitude and depth of slip, as well as source mechanism.

1.2.1 Dependence of Stress Parameter on Magnitude, Mechanism, and Depth of Slip

Conditional on magnitude, earthquakes with predominately deep slip consistently produce larger high-frequency ($f \geq 0.5$ Hz) motions compared to earthquakes with predominately shallow slip (Silva et al. 1996). Consequently, deep-slip earthquakes consistently yield larger estimates of stress parameter when treated as a point-source (e.g. Table 1) and also when modeled as a finite rupture by summing small magnitude (**M** 5.0) subsources (Silva et al. 1996). For earthquakes considered in Silva et al. (1996), the empirical criterion that effectively distinguished between radiation from deep-slip and shallow-slip dominated earthquakes was the percent of moment released above the depth of 5 km. For a given magnitude, shallow-slip dominated earthquakes with more than 20% of moment released above a depth of 5 km showed consistently lower high-frequency motions than deep-slip dominated earthquakes characterized with less than 20% moment released above a depth of 5 km. Moment release was selected rather than the existence of coseismic surface rupture to avoid the ambiguity of earthquakes like Kobe, Japan, which had only very limited coseismic surface rupture, as well as San Fernando and Morgan Hill, CA, which had ambiguities regarding the existence of any coseismic surface rupture.

In the analysis of earthquakes to determine stress parameter reported in this response (Table 1), the effects of deep versus shallow slip are illustrated in Table 2. Considering all 24 earthquakes, the median stress parameter is 28.9 bars with an aleatory variability of 0.59. The shallow-slip and deep-slip dominated earthquakes reflect median estimates of 23.7 bars and 52.0 bars, respectively, a difference of about a factor of two. With the separate treatment of shallow-slip and deep-slip earthquakes, aleatory variability decreased (although a sample of 6 for deep-slip events does not produce a reliable estimate of the standard deviation) (Table 2). This suggests that, when deep-slip and shallow-slip earthquakes are treated together, what is really epistemic variability (deep-slip versus shallow-slip) is included as aleatory variability. The increased knowledge implied by separating earthquakes into deep-slip and shallow-slip classes results in different medians and a more appropriate estimate of the respective aleatory variabilities.

In terms of the static stress drops, Table 2 shows a weak dependence on deep versus shallow slip, 29.7 bars compared to 25.1 bars respectively, about a 20% difference. Aleatory variability for the deep-slip static stress drop (based on only 6 samples) decreased, but shallow-slip static stress drop actually increased relative to the combined data set.

In general, static stress drops do not show clear trends with either magnitude or depth to TOR and suggest a poor correlation with the stress parameters, as seen with the values computed and listed in Table 2 and shown in Figures 1, 2, and 3.

To illustrate the dependence of the stress parameter on magnitude, Figure 4 shows the 24 estimates plotted versus magnitude. There is a general trend of decreasing stress parameter with increasing magnitude, particularly for magnitudes greater than about **M** 7.0. The deep-slip dominated earthquakes reflect the larger median compared to the shallow-slip earthquakes, even over a comparable range in magnitude. A similar plot for static stress drop values is shown in Figure 5 and reveals the lack of clear trends with either magnitude or depth of slip.

Because slip models are not available for future earthquakes, NGA GMPE developers selected depth from the ground surface to the top of rupture (TOR) as a proxy to capture the effects of slip depth on ground motion. As a result, TOR was compiled for all earthquakes for which finite rupture models were available. Figure 6 shows the stress parameters plotted versus depth to TOR and illustrates the distinct difference in expected stress parameter for shallow-slip versus deep-slip dominated earthquakes, as well as the difference in the aleatory variability. This figure also suggests a steep rise in stress parameter between 2 and 3 km depth rather than a gradual increase from the surface, although more data between 2 and 4 km TOR depths would help clarify the transition.

In contrast, Figure 7 shows the static stress drop versus TOR with little visible trends. There appears to be no dependence on TOR and the increased variability over the stress parameter is evident.

1.2.2 Inversion of NGA Ground Motion Prediction Equations

To examine the dependence of the stress parameter on earthquake magnitude, style of faulting, and depth of slip (TOR) in a more systematic manner, median estimates of 5%-damped response spectra from the recent NGA GMPEs (Power et al. 2008) were inverted for point-source

parameters, kappa, Q(f), and stress parameter. The NGA GMPEs analyzed include Abrahamson and Silva (2008), Boore and Atkinson (2008), Campbell and Bozorgnia (2008), and Chiou and Youngs (2008) because these four models included both rock and soil sites characterized by the average shear-wave velocity over the upper 30 m of material ($\overline{\mathbf{V}}_{\mathbf{S}}(30\text{m})$). The analyses consisted of first performing a random-vibration-theory spectral match to the median estimates of 5%-damped response spectra computed from the GMPEs. This process produces Fourier amplitude spectra whose response spectra match those of the target (EPRI 1993; Silva et al. 1996). The resulting Fourier amplitude spectra were then inverted for the desired point-source parameters (EPRI 1993; Silva et al. 1996). For the GMPEs, magnitudes **M** 5.5, **M** 6.5 and **M** 7.5 at a suite of eleven rupture distances were run for rupture mechanisms of strike-slip, normal slip, and reverse slip. For depth to the top of the rupture, two cases were considered. For Case 1, default TORs were taken as magnitude dependent at 6.0, 2.0, and 0.7 km for magnitudes **M** 5.5, **M** 6.5, and **M** 7.5 respectively (Table 3). These default TOR depths are averages based on an analysis of the NGA TOR estimates for magnitude bins **M** 5.00 to 5.99, **M** 6.00 to 6.99, and **M** 7.00 to 7.99. For Case 2, depth to TOR is assumed to be 0.0 km for shallow slip dominated earthquakes and averages 6.8 km for deep slip dominated earthquakes (Table 3). These analyses examined the sensitivity of stress parameter to deep slip versus shallow slip.

Results of the analyses on the four NGA GMPEs are summarized in Table 4 for Case 1. For this case, inversions were performed for both rock and soil sites with $\overline{\mathbf{V}}_{\mathbf{S}}(30\text{m})$ = 550m/sec and 270m/sec respectively and with appropriate amplification (Silva et al. 1996). The GMPE predictions were computed using the default magnitude dependent TOR (Table 4) as well as default depths to 1.0 km/sec and 2.5 km/sec material for the specific $\overline{\mathbf{V}}_{\mathbf{S}}(30\text{m})$. The resulting stress parameters show a strong magnitude dependence as well as a large increase (about 30% overall) in stress parameter for reverse mechanism compared to normal and strike slip mechanisms, which were about equal. The strong magnitude dependence is consistent with previous analyses of pre-NGA GMPEs (EPRI 1993; Boore and Joyner 1997; Silva et al. 1996) as well as empirical analyses based directly on strong motion recordings (Atkinson and Silva 1997). The strong dependence of the stress parameter on magnitude, especially for **M** > 6.5 has been interpreted as the potential effects of saturation due to source finiteness (Atkinson and Silva 1997). In some studies, stress parameter dependencies have been accommodated through modification of the source model. Examples include addition of a second corner frequency (Atkinson and Silva 1997), changing the stress parameter with magnitude (EPRI 2004), and adding a depth term that increases with magnitude (EPRI 2004). This magnitude dependence of the stress parameter is stronger than previous analyses suggest, likely due to the effects of slip depth through the TOR dependence on magnitude, not previously accommodated as an independent parameter.

For Case 2, as a first step, inversions were performed for rock sites only. Results are summarized in Table 5 for shallow slip (TOR=0.0 km), deep slip (TOR=6.8 km) and default slip (TOR varies with magnitude) for strike-slip, normal, and reverse faulting mechanisms. Because Case 2 was run for only rock sites, stress parameter results for default slip differ from those in Case 1, which was run for rock and soil sites. However, the trends are quite similar, suggesting the stress parameter dependencies with deep slip and shallow slip dominated ruptures is stable. In general, deep slip cases show about a 30% increase in stress parameter versus shallow-slip

cases across mechanism (Table 5). This is less than the roughly 100% shown in the suite of 24 NGA earthquakes (Table 2), with the difference likely due to a combination of sample size (only six deep slip-dominated earthquakes of the 24 available) as well as the effect of faulting mechanism not being distinguished in the earthquake analysis (Table 2), due to too few data with deep slip.

The stress parameter analyses of the NGA GMPEs reveal a strong magnitude dependency and a strong dependency with faulting mechanism, with reverse faulting having stress parameters about 30% greater than normal and strike-slip ruptures. Additionally, the effects of deep versus shallow slip also show about a 30% effect with deep slip-dominated earthquakes resulting in larger stress parameters than shallow slip-dominated earthquakes of the same magnitude.

Section 1.2.3 Summary

Based on an updated analysis of recorded earthquakes, median static stress drop is found to be approximately equal to median stress parameter (point-source stress drop). This result revises the observation in the responses to RAI 3.2.2.1.2.1-2-019 and Supplemental Question 6, based on earlier analyses, that static stress drop is approximately half the point-source stress drop. The earlier result reflected the distribution of magnitude, rupture mechanism, and slip depth that characterized the more limited strong motion data set available prior to the recent NGA project.

Theoretical considerations show that static stress drop and stress parameter have an equivalent dependence on moment and corner frequency that is related to the finite nature of the fault rupture area. Stress parameter, however, depends more on the dynamics of rupture and shows a stronger correlation to the level of strong ground motion. To demonstrate consistency of the screening evaluation for FEP 1.2.10.01.0A, *Hydrologic Response to Seismic Activity*, with levels of ground motion developed for seismic analyses (i.e., relate water table rise to ground motion level) requires consideration of both the stress parameter (point-source stress drop) and static stress drop, and the relation between them. As discussed in the response to Supplemental Question 5, demonstration of consistency between the screening evaluation and the characterization of seismic sources in the PSHA was accomplished through consideration of static stress drop alone.

Implications of the revised relation between static stress drop and stress parameter (point-source stress drop) are discussed in Section 1.2.3 of the response to Supplemental Question 5. The screening evaluation for FEP 1.2.10.01.0A, *Hydrologic Response to Seismic Activity*, is consistent with the updated results and conclusions of these seismic analyses.

Table 1. NGA Earthquake Data Summary

EQID	EQNAME	Date (year)	Date (MODY)	Mag	Mech[1]	Slip Depth[2] (S=Shallow, D=Deep)	TOR[3] (km)	Rupture Length (km)	Rupture Width (km)	Rupture Area (km × km)	Static Stress Drop (bars)	Stress Parameter (bars)[5]
0006	Imperial Valley-02	1940	0519	6.95	0		0.0	63.0	13.0	818.8	31.04	
0012	Kern County	1952	0721	7.36	2		0.0	64.7	17.0	1098.6	82.31	
0025	Parkfield	1966	0628	6.19	0		0.0	24.9	12.0	299.0	10.19	
0028	Borrego Mtn	1968	0409	6.63	0		0.0	30.0	12.0	360.1	35.24	
0030	San Fernando	1971	0209	6.61	2	S	0.0	16.0	27.4	438.5	24.48	40.2
0031	Managua, Nicaragua-01	1972	1223	6.24	0		2.0	11.5	6.0	69.0	109.25	
0040	Friuli, Italy-01	1976	0506	6.50	2		2.3	13.0	13.7	178.0	64.73	
0041	Gazli, USSR	1976	0517	6.80			3.8	22.5	17.0	382.6	57.89	
0043	Friuli, Italy-02	1976	0915	5.91	2		1.0	4.9	8.3	40.7	77.15	
0045	Santa Barbara	1978	0813	5.92	3		11.6	10.0	5.0	50.0	58.65	
0046	Tabas, Iran	1978	0916	7.35	2	S	1.0	90.0	35.0	3,149.6	16.38	10.2
0048	Coyote Lake	1979	0806	5.74	0	D	3.1	6.6	7.0	46.2	35.46	59.5
0050	Imperial Valley-06	1979	1015	6.53	0	S	0.0	50.0	13.0	649.9	10.29	32.7
0056	Mammoth Lakes-01	1980	0525	6.06	4		1.3	15.0	10.0	150.0	18.30	
0057	Mammoth Lakes-02	1980	0525	5.69	0		9.0	10.0	6.0	60.0	20.16	
0064	Victoria, Mexico	1980	0609	6.33	0		4.0	30.0	10.0	300.0	16.44	
0068	Irpinia, Italy-01	1980	1123	6.90	1		0.0	47.0	15.0	705.0	32.69	
0069	Irpinia, Italy-02	1980	1123	6.20	1		0.0	15.0	10.1	151.5	29.25	
0072	Corinth, Greece	1981	0224	6.60	1		0.0	37.0	13.0	481.0	20.58	
0073	Westmorland	1981	0426	5.90	0		2.0	10.0	7.0	70.0	33.04	
0076	Coalinga-01	1983	0502	6.36	2		3.4	16.0	11.0	176.0	40.59	
0083	Ierissos, Greece	1983	0806	6.70	0		1.0	42.0	14.0	588.2	21.50	
0087	Borah Peak, ID-01	1983	1028	6.88	1		0.0	41.0	20.3	832.5	23.78	
0090	Morgan Hill	1984	0424	6.19	0	S	0.5	27.0	11.5	310.5	9.63	24.1
0091	Lazio-Abruzzo, Italy	1984	0507	5.80	1		8.0	6.0	8.1	48.6	40.43	
0096	Drama, Greece	1985	1109	5.20	4		0.0	10.0	12.0	120.0	1.31	
0097	Nahanni, Canada	1985	1223	6.76	2	S	2.0	33.6	17.6	591.5	26.23	25.4
0101	N. Palm Springs	1986	0708	6.06	3	D	4.0	20.0	13.3	266.1	7.75	60.8

Table 1. NGA Earthquake Data Summary (continued)

EQID	EQNAME	Date (year)	Date (MODY)	Mag	Mech[1]	Slip Depth[2] (S=Shallow, D=Deep)	TOR[3] (km)	Rupture Length (km)	Rupture Width (km)	Rupture Area (km × km)	Static Stress Drop (bars)	Stress Parameter (bars)[5]
0102	Chalfant Valley-01	1986	0720	5.77	0		2.0	7.5	6.0	45.0	40.92	
0103	Chalfant Valley-02	1986	0721	6.19	0		4.0	15.0	8.0	119.9	40.13	
0108	San Salvador	1986	1010	5.80	0		5.9	8.0	7.0	56.0	32.69	
0111	New Zealand-02	1987	0302	6.60	1		0.0	13.0	10.2	132.6	142.20	
0113	Whittier Narrows-01	1987	1001	5.99	3	D	14.5	10.0	6.0	60.0	56.82	53.1
0115	Superstition Hills-01	1987	1124	6.22	0		0.0	20.0	10.0	200.0	20.66	
0116	Superstition Hills-02	1987	1124	6.54	0	S	0.0	20.0	12.0	240.0	47.47	18.4
0118	Loma Prieta	1989	1018	6.93	3	D	3.8	40.0	18.0	719.8	35.15	51.3
0119	Griva, Greece	1990	1221	6.10	1		0.0	17.5	16.0	280.0	8.24	
0121	Erzican, Turkey	1992	0313	6.69	0		3.7	29.0	8.0	232.1	83.79	
0123	Cape Mendocino[4]	1992	0425	7.01	2	D	5.2	20.0	28.0	559.7		
0125	Landers	1992	0628	7.28	0	S	0.0	71.7	15.0	1075.1	64.50	40.7
0127	Northridge-01	1994	0117	6.69	2	D	5.0	18.0	24.0	432.1	32.99	53.8
0128	Double Springs	1994	0912	5.90	0		3.0	10.0	7.0	70.0	33.04	
0129	Kobe, Japan	1995	0116	6.90	0	S	0.2	60.0	20.0	1199.9	14.72	34.9
0130	Kozani, Greece-01	1995	0513	6.40	1		2.8	27.0	15.7	424.0	12.46	
0134	Dinar, Turkey	1995	1001	6.40	1		0.0	12.6	13.3	167.5	50.20	
0135	Gulf of Aqaba	1995	1122	7.20	0		1.0	54.0	25.0	1349.8	34.78	
0136	Kocaeli, Turkey	1999	0817	7.51	0	S	0.0	137.5	20.2	2784.0	34.25	14.7
0137	Chi-Chi, Taiwan	1999	0920	7.62	3	S	0.0	88.0	40.2	3,539.0	34.94	13.9
0138	Duzce, Turkey	1999	1112	7.14	0	S	0.0	46.8	20.3	948.9	47.96	8.2
0140	Sitka, Alaska	1972	0730	7.68	0		0.0	180.0	15.0	2,700.0	64.51	
0141	Caldiran, Turkey	1976	1124	7.21			2.0	55.0	18.0	990.0	57.31	
0142	St Elias, Alaska	1979	0228	7.54	2		0.0	56.1	70.4	3,948.0	22.50	
0144	Manjil, Iran	1990	0620	7.37	0		0.0	71.6	16.0	1,145.8	79.99	
0145	Sierra Madre	1991	0628	5.61	2		10.0	4.3	3.9	16.8	103.21	
0152	Little Skull Mtn, NV	1992	0629	5.65	1	D	6.4	6.0	6.0	36.0	37.78	37.2
0158	Hector Mine	1999	1016	7.13	0	S	0.0	69.0	16.2	1,117.9	36.23	24.8

Table 1. NGA Earthquake Data Summary (continued)

EQID	EQNAME	Date (year)	Date (MODY)	Mag	Mech[1]	Slip Depth[2] (S=Shallow, D=Deep)	TOR[3] (km)	Rupture Length (km)	Rupture Width (km)	Rupture Area (km × km)	Static Stress Drop (bars)	Stress Parameter (bars)[5]
0168	Nenana Mountain, Alaska	2002	1023	6.70	0		0.1	30.0	15.0	450.0	32.13	
0169	Denali, Alaska	2002	1103	7.90	0	S	0.0	326.7	15.6	5085.3	53.36	12.0
0171	Chi-Chi, Taiwan-02	1999	0920	5.90	2	D	6.5	19.0	13.0	247.0	5.00	55.0
0172	Chi-Chi, Taiwan-03	1999	0920	6.20	2	D	6.7	10.0	11.0	110.0	47.30	30.0
0173	Chi-Chi, Taiwan-04	1999	0920	6.20	0	S	1.5	21.5	17.5	376.3	7.50	53.3
0174	Chi-Chi, Taiwan-05	1999	0922	6.20	2	D	7.7	17.5	19.0	332.4	9.00	218.0
0175	Chi-Chi, Taiwan-06	1999	0925	6.30	2	D	10.0	29.0	20.0	580.0	5.50	80.9
0179	Parkfield	2004	0929	6.00	0	S	0.5	40.0	15.0	600.0	1.86	20.2
0177	San Simeon	2003	1222	6.50	2	S	2.0	33.0	10.0	330.0	25.64	34.0
0178	Bam, Iran	2003	1226	6.50	0	S	1.4	12.0	8.6	103.2	146.62	47.2
0176	Tottori	2000	1006	6.60	0	S	1.0	34.0	17.6	598.4	14.83	49.9
0180	Niigata	2004	1023	6.60	2	S	0.0	24.0	16.0	384.0	28.85	32.5

Source: NGA database. Stress parameter values were determined as part of this analysis.

NOTES:

[1]Mechanism	Mechanism ID	Rake Angles
Strike -Slip	0	−180 < Rake < −150; −30 < Rake < 30; 150 < Rake < 180
Normal	1	−120 < Rake < −60
Reverse	2	60 < Rake < 120
Reverse – Oblique	3	30 < Rake < 60
		120 < Rake < 150
Normal – Oblique	4	−150 < Rake < −120
		−60 < Rake < −30

[1]Faulting mechanism assigned according to rake angle.

[2]Depth from ground surface to Top of Rupture.

[3]Shallow Slip, 20% or more of moment released at depths above 5 km; Deep Slip, less than 20% of moment released at depths above 5 km.

[4]Disputed classification as a crustal or subduction related earthquake.

[5] The data processing and inversions were performed by Dr. Yun of KEPRI, a Korea-based government research facility. Stress parameter estimates, while preliminary, are considered appropriate for their intended use to investigate the potential dependence on magnitude and depth of slip as well as correlation with the static stress drop.

Table 2. Comparison of Static Stress Drops and Stress Parameters

Slip	$\Delta\sigma_{static}$ (bars)	σ_{ln}	Number of Earthquakes	$\Delta\sigma_{SP}$ (bars)	σ_{ln}	Number of Earthquakes	Correlation[1]
NGA Earthquakes with Finite Rupture Models							
All	30.6	0.86	62				
NGA Earthquakes With Stress Parameters (preliminary estimates)							
All Slip	26.2	0.87	24	28.9	0.59	24	0.0
Shallow Slip	25.1	0.94	18	23.7	0.54	18	-0.1
Deep Slip	29.7	0.69	6	52.0	0.18	6	-0.6

[1] Correlation between static stress drops and stress parameters determined using the Spearman's rank correlation coefficient.

Table 3. Top-of-Rupture for Inversion of NGA GMPEs

	Depth of Top of Rupture (km)		
Moment Magnitude	Default	Shallow Slip	Deep Slip
5.5	6.0	0.0	6.8
6.5	2.0	0.0	6.8
7.5	0.7	0.0	6.8

Table 4. Stress Parameters Based On Inversions of NGA GMPEs: Case 1

Includes Rock ($\overline{V}_S$ (30m) = 550m/s) and Soil Sites ($\overline{V}_S$ (30m) = 270m/s), Default TOR (M)			
M	$\Delta\sigma_{SP}$ (bars) Strike Slip	$\Delta\sigma_{SP}$ (bars) Normal [1]	$\Delta\sigma_{SP}$ (bars) Reverse[1]
5.5	66.1	62.8	86.4
6.5	45.8	39.2	55.4
7.5	23.8	22.4	28.9
Median	41.6	38.0	51.7

NOTES: [1] 45° dip, sites not hanging wall, not foot wall.

Table 5. Stress Parameters Based On Inversions of NGA GMPEs: Case 2

Rock Sites Only [2] ($\overline{V}_S$ (30m) = 550m/s)									
	$\Delta\sigma_{SP}$ (bars) Strike Slip			$\Delta\sigma_{SP}$ (bars) Normal [1]			$\Delta\sigma_{SP}$ (bars) Reverse [1]		
M	Shallow	Deep	Default	Shallow	Deep	Default	Shallow	Deep	Default
5.5	46.6	59.0	57.6	45.4	58.0	56.1	54.4	69.7	67.9
6.5	43.9	57.8	49.4	41.9	55.8	44.4	49.8	66.4	52.8
7.5	33.9	45.9	35.2	33.2	44.1	33.6	37.5	51.2	39.1
Median	41.1	53.9	46.4	39.8	52.2	43.7	46.7	61.9	52.0

NOTES:

[1] 45° dip, sites not hanging wall, not foot wall.

[2] Inversions distinguishing between deep slip and shallow slip were carried out only for rock site conditions. Thus, default TOR results differ between Table 4 (rock and soil) and this table (rock only).

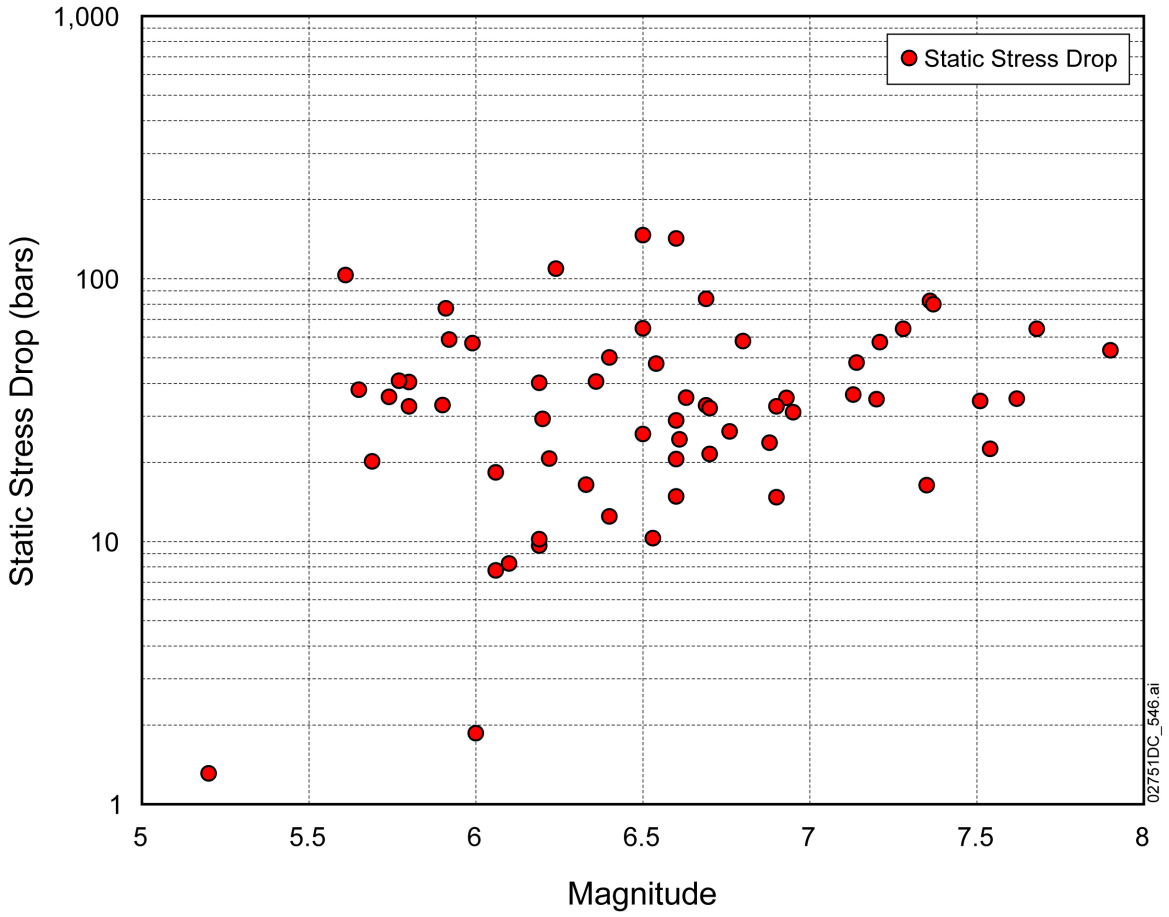

Source: Table 1.

Figure 1. Estimates of Static Stress Drops (circular rupture) versus Magnitude (M)

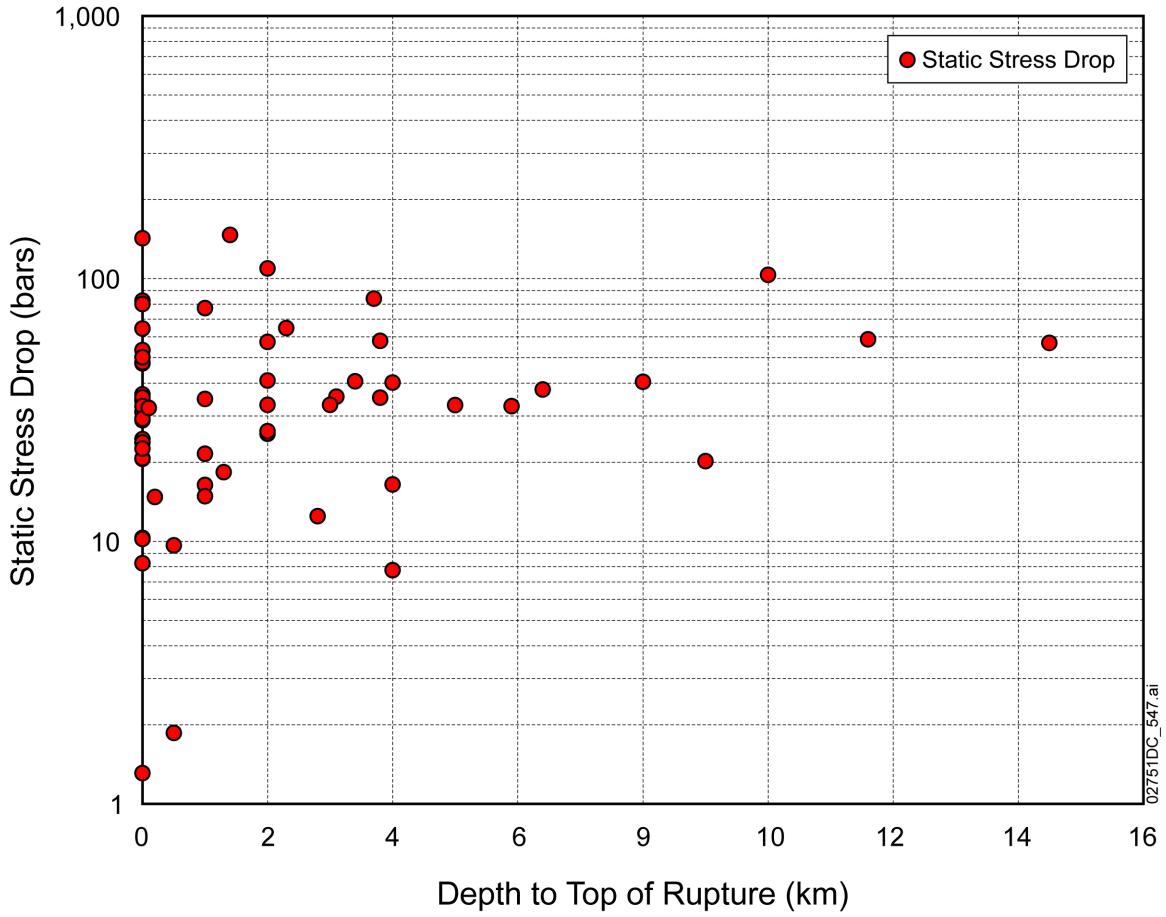

Source: Table 1.

Figure 2. Estimates of Static Stress Drops (circular rupture) versus Depth to Top-of-Rupture (TOR)

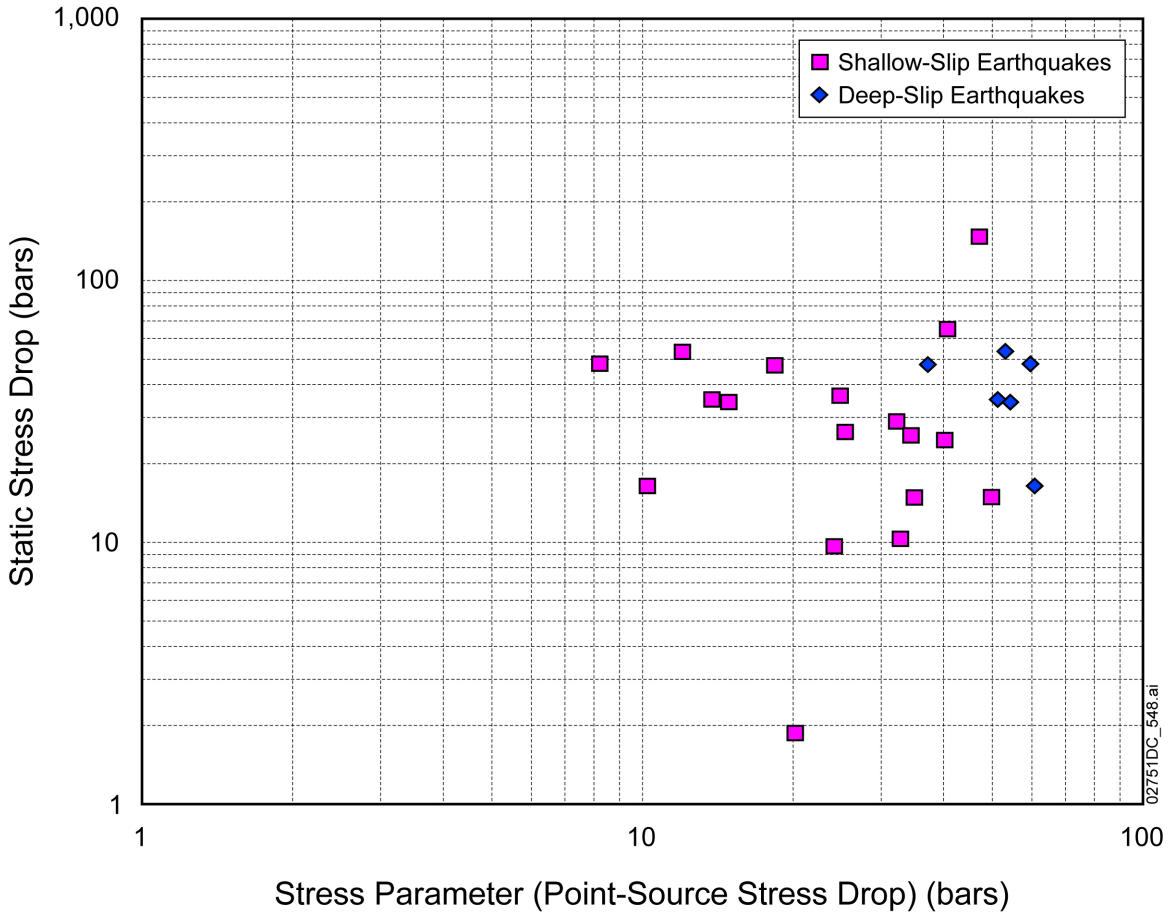

Source: Table 1.

NOTES: Squares represent shallow slip earthquakes (20% or more moment release above 5 km depth); diamonds represent deep slip earthquakes (less than 20% moment release above 5 km depth).

Figure 3. Estimates of Stress Parameter versus Static Stress Drop

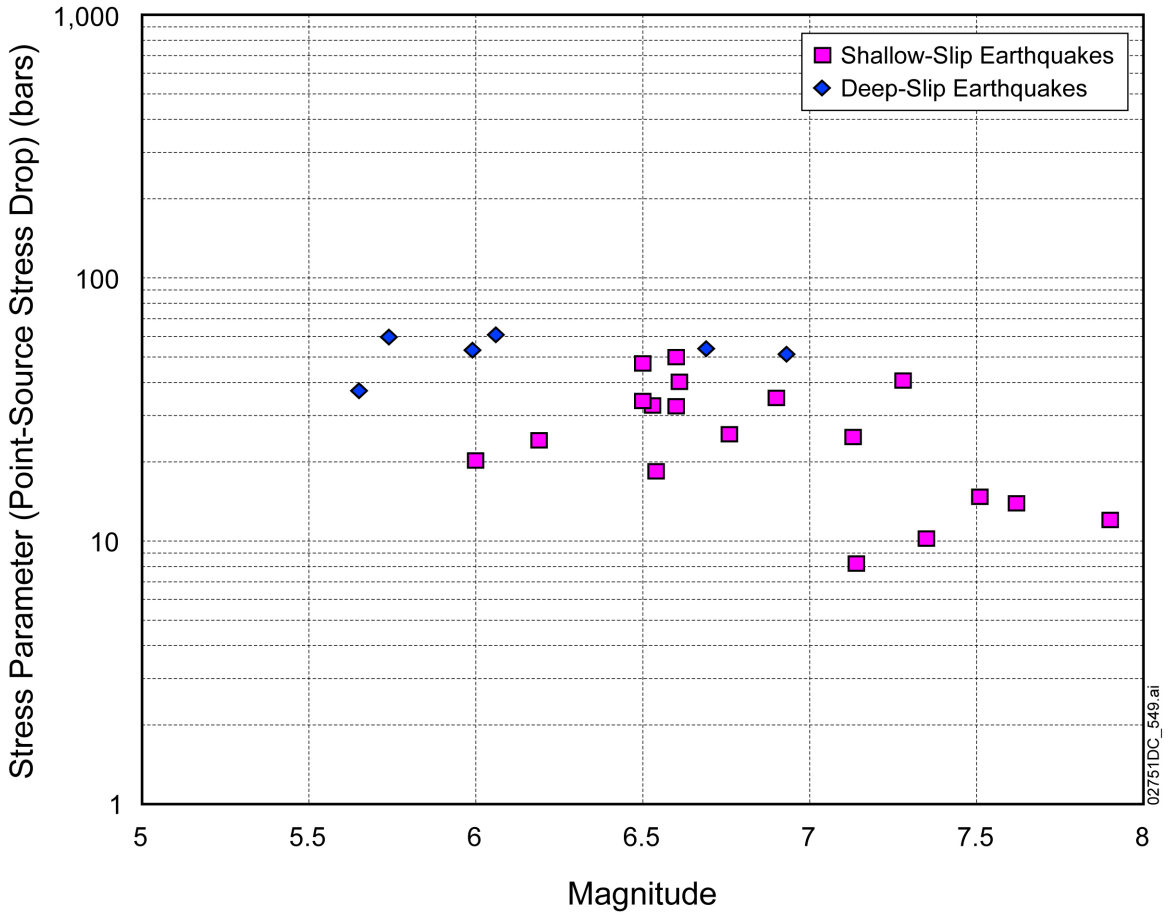

Source: Table 1.

NOTES: Squares represent shallow slip earthquakes (20% or more moment release above 5 km depth); diamonds represent deep slip earthquakes (less than 20% moment release above 5 km depth).

Figure 4. Estimates of Stress Parameter versus Magnitude (**M**)

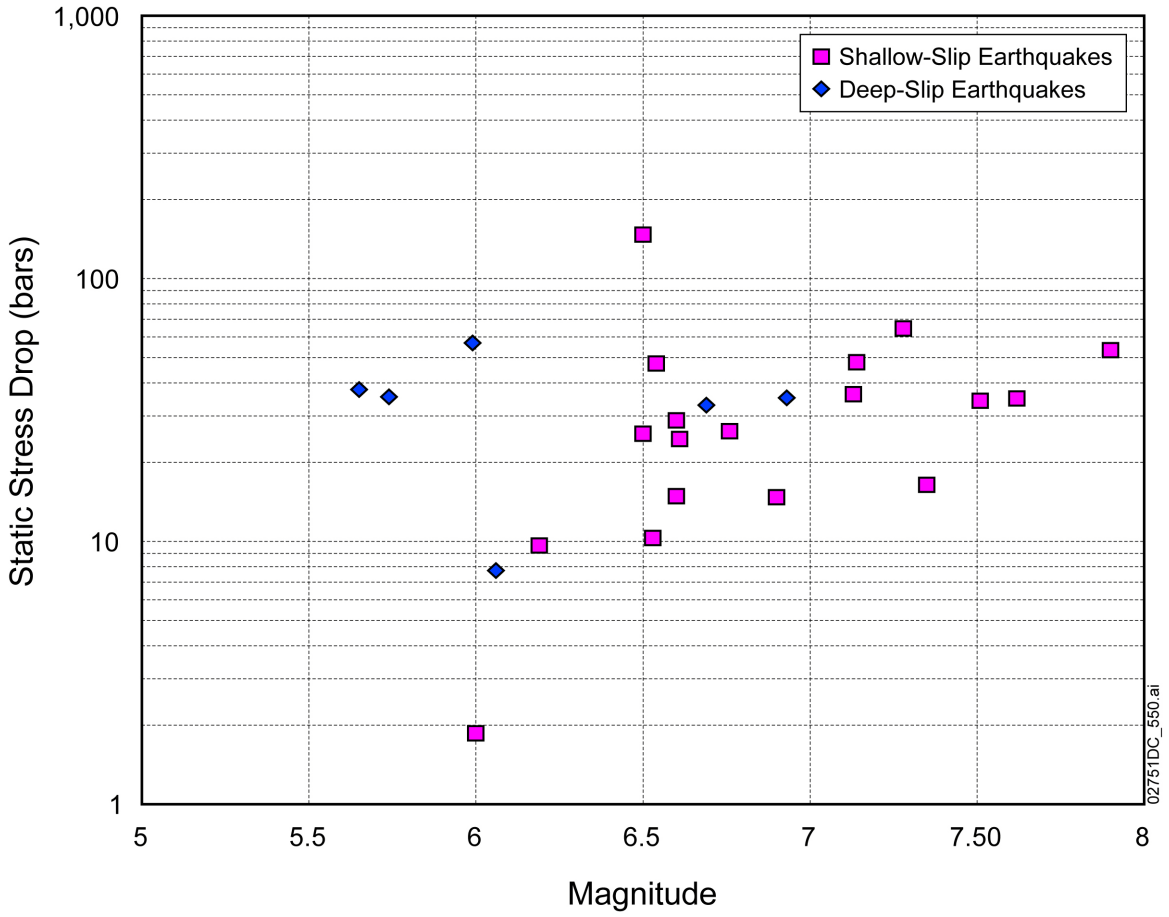

Source: Table 1.

NOTES: Squares represent shallow slip earthquakes (20% or more moment release above 5 km depth); diamonds represent deep slip earthquakes (less than 20% moment release above 5 km depth).

Figure 5. Estimates of Static Stress Drop versus Magnitude (**M**)

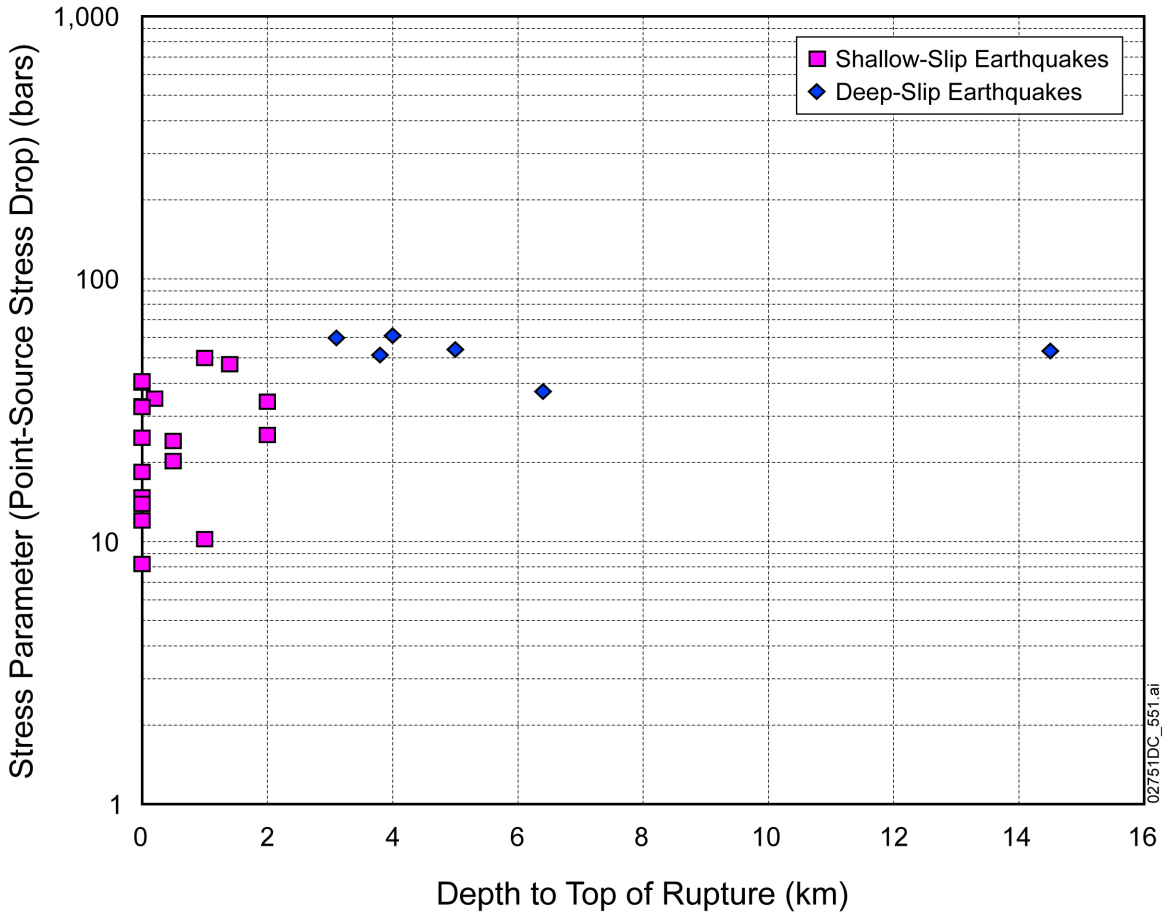

Source: Table 1.

NOTES: Squares represent shallow slip earthquakes (20% or more moment release above 5 km depth); diamonds represent deep slip earthquakes (less than 20% moment release above 5 km depth).

Figure 6. Estimates of Stress Parameter versus Depth to Top-of-Rupture

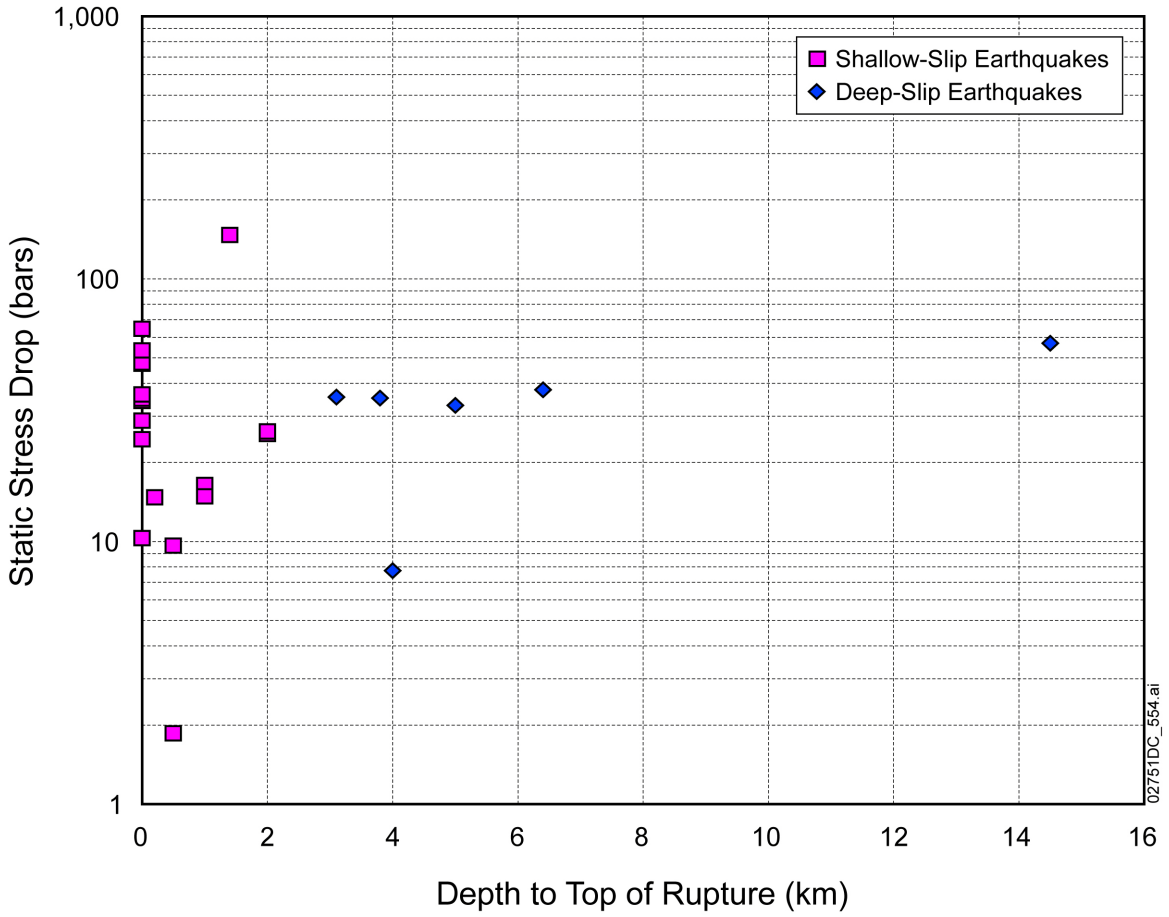

Source: Table 1.

NOTES: Squares represent shallow slip earthquakes (20% or more moment release above 5 km depth); diamonds represent deep slip earthquakes (less than 20% moment release above 5 km depth).

Figure 7. Estimates of Static Stress Drop versus Depth to Top-of-Rupture

2. COMMITMENTS TO NRC

None.

3. DESCRIPTION OF PROPOSED LA CHANGE

None.

4. REFERENCES

Abrahamson, N. and Silva, W. 2008. "Summary of the Abrahamson & Silva NGA Ground-Motion Relations." *Earthquake Spectra, 24*, (1), 67-97. Oakland, California: Earthquake Engineering Research Institute.

Abrahamson, N.A. and Shedlock, K.M. 1997. "Overview." *Seismological Research Letters, 68*, (1), 9-23. El Cerrito, California: Seismological Society of America.

Aki, K. and Richards, P.G. 1980. *Quantitative Seismology, Theory and Methods*. Two volumes. San Francisco, California: W.H. Freeman and Company.

Atkinson, G.M. and Silva, W. 1997. "An Empirical Study of Earthquake Source Spectra for California Earthquakes." *Bulletin of the Seismological Society of America, 87*, (1), 97-112. El Cerrito, California: Seismological Society of America.

Brune, J.N. 1970. "Tectonic Stress and the Spectra of Seismic Shear Waves from Earthquakes." *Journal of Geophysical Research, 75*, (26), 4997-5009. Washington, D.C.: American Geophysical Union.

Brune, J.N. 1971. "Tectonic Stress and the Spectra of Seismic Shear Waves from Earthquakes [Correction]." *Journal of Geophysical Research, 76*, (20), 5002. Washington, D.C.: American Geophysical Union.

Boore, D.M. and Atkinson, G.M. 2008. "Ground-Motion Prediction Equations for the Average Horizontal Component of PGA, PGV, and 5%-Damped PSA at Spectral Periods between 0.01 s and 10.0 s." *Earthquake Spectra, 24*, (1), 99-138. Oakland, California: Earthquake Engineering Research Institute.

Boore, D.M. and Joyner, W.B. 1997. "Site Amplifications for Generic Rock Sites." *Bulletin of the Seismological Society of America, 87*, (2), 327-341. El Cerrito, California: Seismological Society of America.

Campbell, K.W. and Bozorgnia, Y. 2008. "NGA Ground Motion Model for the Geometric Mean Horizontal Component of PGA, PGV, PGD and 5% Damped Linear Elastic Response Spectra for Periods Ranging from 0.01 to 10 s." *Earthquake Spectra, 24*, (1), 139-171. Oakland, California: Earthquake Engineering Research Institute.

Chiou, B., Darragh, R., Gregor, N. and Silva, W. 2008. "NGA Project Strong-motion Database." *Earthquake Spectra, 24*, (1), 23-44. Oakland, California: Earthquake Engineering Research Institute.

Chiou, B.S.-J. and Youngs, R.R. 2008. "An NGA Model for the Average Horizontal Component of Peak Ground Motion and Response Spect." *Earthquake Spectra, 24*, (1), 173-215. Oakland, California: Earthquake Engineering Research Institute.

EPRI (Electric Power Research Institute) 2004. *CEUS Ground Motion Project Final Report.* Report 1009684. Palo Alto, California: Electric Power Research Institute.

EPRI (Electric Power Research Institute) 1993. *Method and Guidelines for Estimating Earthquake Ground Motion in Eastern North America*. Five volumes. EPRI TR-102293. Palo Alto, California: Electric Power Research Institute.

Heaton, T.H. 1990. "Evidence for and Implications of Self-healing Pulses of Slip in Earthquake Rupture". *Physics of the Earth and Planetary Interiors, 64*, 1-20. Amsterdam, The Netherlands: Elsevier.

Power, M.; Chiou, B.; Abrahamson, N.; Bozorgnia, Y.; Shantz, T.; and Roblee, C. 2008. "An Overview of the NGA Project." Earthquake *Spectra, 24*, (1), 3-21. Oakland, California: Earthquake Engineering Research Institute.

Silva, W.J.; Abrahamson, N.; Toro, G.; and Costantino, C. 1996. *Description and Validation of the Stochastic Ground Motion Model*. PE&A 94PJ20. El Cerrito, California: Pacific Engineering and Analysis.

Wells, D.L. and Coppersmith, K.J. 1994. "New Empirical Relationships Among Magnitude, Rupture Length, Rupture Width, Rupture Area, and Surface Displacement." *Bulletin of the Seismological Society of America, 84*, (4), 974-1002. El Cerrito, California: Seismological Society of America.